NUMERICAL ANALYSES OF FLOW CHARACTERISTICS IN THE VICINITY OF SPILLWAY AERATORS

A THESIS SUBMITTED TO
THE GRADUATE SCHOOL OF NATURAL AND APPLIED SCIENCES
OF
MIDDLE EAST TECHNICAL UNIVERSITY

BY

CAN KURT

IN PARTIAL FULFILLMENT OF THE REQUIREMENTS
FOR
THE DEGREE OF MASTER OF SCIENCE
IN
CIVIL ENGINEERING

APRIL 2016

Approval of the thesis:

NUMERICAL ANALYSES OF FLOW CHARACTERISTICS IN THE VICINITY OF SPILLWAY AERATORS

submitted by **CAN KURT** in partial fulfillment of the requirements for the degree of **Master of Science in Civil Engineering Department, Middle East Technical University** by,

Prof. Dr. Gülbin Dural Ünver
Dean, Graduate School of **Natural and Applied Sciences** _____

Prof. Dr. İsmail Özgür Yaman
Head of Department, **Civil Engineering** _____

Asst. Prof. Dr. Talia Ekin Tokyay Sinha
Supervisor, **Civil Engineering Department, METU** _____

Examining Committee Members:

Prof. Dr. Burcu Altan Sakarya
Civil Engineering Dept., METU _____

Asst. Prof. Dr. Talia Ekin Tokyay Sinha
Civil Engineering Dept., METU _____

Assoc .Prof. Dr. Yakup Darama
Civil Engineering Dept., Atılım Univesity _____

Asst. Prof. Dr. Melih Çalamak
Civil Engineering Dept., TED University _____

Asst. Prof. Dr. Nuray Öktem
Mathematics Dept., Çanakkale Onsekiz Mart University _____

Date: **25.04.2016**

I hereby declare that all information in this document has been obtained and presented in accordance with academic rules and ethical conduct. I also declare that, as required by these rules and conduct, I have fully cited and referenced all material and results that are not original to this work.

Name, Last name: Can KURT

Signature :

ABSTRACT

NUMERICAL ANALYSES OF FLOW CHARACTERISTICS IN THE VICINITY OF SPILLWAY AERATORS

Kurt, Can

M.S., Department of Civil Engineering

Supervisor: Asst. Prof. Dr. Talia Ekin Tokyay Sinha

April 2016, 80 pages

Spillway aerators are used in the spillways that are designed to carry medium to high discharges during their operation. Aerators are aimed to reduce the risk of cavitation in these high velocity flows. Most of the time, design of these aerators are based on physical models and experimental results. However, with the advancement in computational resources, it became possible to analyze the effect of aerators using computational fluid dynamics (CFD). To this end, three-dimensional numerical simulations of such flows are conducted using finite-volume techniques. In this study the k-ε model is used for turbulence closure and the air-water interface tracking is made possible using Volume of Fluid (VOF) method. The aim of the study is to quantify the effect of submerged circular aerators located at the bottom of a stepped spillway to the flow structure in general. A single sloped ($\tan(\theta)=0.3$) spillway with single step is considered in the study. The flow enters the step over a small ramp called a deflector. The ramp angle is considered as one of the variables in the test cases. Two different ramp angles are considered and the results are compared to a step without any ramp. Discharge of the flow over the spillway, the aerator number, size and position with respect to one another, Froude number are considered as other

variables in the study. The jet-length, amount of air-entrainment, average flow structure after the step are investigated.

Through numerical simulations a direct relation between jet-length and $Fr^{1.75}$ is observed. Varying the location of the aerators over the step do not change the overall aeration significantly. However, larger diameter aerators that are placed closely together might affect the air concentration near the channel bed. A logarithmic decay of air concentration in the streamwise direction after the reattachment point is observed through simulations.

Keywords: CFD, Spillway aerators, Ansys Fluent, Cavitation

ÖZ

DOLUSAVAK HAVALANDIRICILARININ CİVARINDA AKIM KARAKTERİSTİKLERİNİN SAYISAL YÖNTEMLERLE İNCELENMESİ

Kurt, Can

Yüksek Lisans, İnşaat Mühendisliği Bölümü

Tez Yöneticisi: Yrd. Doç. Dr. Talia Ekin Tokyay Sinha

Nisan 2016, 80 sayfa

Dolusavak havalandırıcıları, orta ve yüksek debili akımların geçmesi planlanarak tasarlanmış dolusavaklarda bulunurlar. Havalandırıcıların amacı yüksek hızlı akımlarda oluşabilecek kavitasyon hasarını önlemektir. Bu havalandırıcıların tasarımları çoğu zaman fiziksel modellere ve deneysel sonuçlara dayandırılarak yapılmıştır. Günümüzde gelişmiş sayısal hesap yöntemleri, havalandırıcı etkilerinin Hesaplamalı Akışkanlar Dinamiği (HAD) kullanılarak analiz edilmesini mümkün kılmıştır. Bu gelişmeler sonucunda sonlu hacimler tekniği kullanılarak bu gibi akımların 3 boyutlu sayısal modellerinin yürütülmesi sağlanmıştır. Bu çalışmada türbülans yakınsaması için k-ε model, hava-su arasındaki etkileşimi gözlemlemek için ise Akışkan Hacimleri Yöntemi (VOF) kullanılmıştır. Bu çalışmanın amacı dolusavak üzerindeki bir basamağın tabanına konumlandırılacak olan dairesel havalandırıcıların akım ve yapı üzerindeki etkilerini gözlemlemektir. Bu sebeple tek eğimli ($\tan(\theta)=0.3$) ve tek basamağa sahip bir dolusavak modeli inclenmiştir. Akım bu basamağa küçük bir rampa olan saptırıcıdan geçerek giriş yapmaktadır. Bu saptırıcının açısı çalışmadaki değişkenlerden birini oluşturmaktadır. İki adet farklı açıya sahip rampalar oluşturulmuş ve rampa olmaması durumu da incelenerek

karşılaştırmalar yapılmıştır. Dolusavaktaki akım debisi, havalandırıcıların adedi, boyutları ve dizilimler ile Froude sayısı bu çalışmadaki diğer değişkenlerdir. Havlandırıcılardan geçen akımın jet uzunluğu, hava alma mekanizması ve ortalama akım yapısı incelenmiştir.

Sayısal simülasyonlar doğrultusunda jet uzunluğu ve $Fr^{1.75}$ fonksiyonu arasında doğrudan bir bağıntı olduğu gözlenmiştir. Havalandırıcı dizilim şekillerinin akımın havalandırılmasında önemli bir etkisi olmadığı sonucuna ulaşılmıştır. Bununla birlikte daha büyük alana sahip havalandırıcıların daha sık olarak yerleştirilmesinin kanal tabanındaki havalandırmaya etkisi olabileceği düşünülmektedir. Ayrıca simülasyonlar sonucu, jetin kanala çarpma noktasından sonra, akım içerisindeki hava konsantrasyonunun akım yönünde logaritmik bir düşüş sergilediği gözlenmiştir.

Anahtar Kelimeler: HAD, Dolusavak havalandırıcıları, Ansys Fluent, Kavitasyon

To My Wife…

ACKNOWLEDGEMENTS

I would like to express my special appreciation and thanks to my advisor Asst. Prof. Dr. Talia Ekin Tokyay Sinha who has supported me for my graduate studies and shared her wealth of knowledge. Without her guidance and encouragement this study would have not been possible.

I would also like to thank my committee members, Prof. Dr. Burcu Altan Sakarya, Assoc. Prof. Dr. Yakup Darama, Asst. Prof. Dr. Melih Çalamak and Asst. Prof. Dr. Nuray Öktem for their creative comments and suggestions and granting an extension of time for finalizing my studies.

I deeply thank to my younger brother Onat. We made many great memories together in this period as in our lifetime. The moments we spend together are invaluable.

Many thanks must go to my parents, Harun and Gülsemin Kurt, for their unconditional trust, constant encouragement, everlasting patience and most importantly for endless love through all my life.

I would like to express my gratitude to my parents-in-law, Saffet and Nuray Topcuoğlu, for their unfailing emotional support.

I would also like to present my thanks to my roommate Cemal İlhan for making the moments valuable at work and to Tolga Şentürk for believing in me and his endless support. I would also like to thank whole Statica Team: Altuğ Aksaray, Hakan Bayram, Eser Reyhanoğulları, İpek Koyuncu, Türköz Gargun, Cankut Er, Ferit Yalçın, Kemal Kaya, Kerem Yayla and Arzu Çeltikoğlu.

I would like to express my special thanks to my friends; Cem Mansız for being with me in all my unforgettable moments, Itır Gevrek for her priceless friendship who we start together to this journey and will finalize at the same time, Melike Helvacıoğlu

for welcoming us every time and everywhere, Açelya Ecem Yıldız for her visits with nice conversation and Ali Ersin Dinçer for making the times in department enjoyable.

Last, but not least, I would like to thank my wife Buse for her amaranthine love and understanding. She has always stood beside me in this 6 year period. Without her moral support and effort I would not have come to this point. She is my rock and I dedicate this study to her.

TABLE OF CONTENTS

LIST OF FIGURES

FIGURES

LIST OF TABLES

TABLES

LIST OF SYMBOLS

A_a	Total area of air inlet
A_w	Area of flow over ramp or step
A_1	Integration constant by Chanson (2013)
A_2	Integration constant for present study
B_1	Air diffusivity constant by Chanson (2013)
B_2	Air diffusivity constant for present study
C_{air}	Air concentration
$C_{1\varepsilon}$	Constant offered by Launder and Spalding (1972)
$C_{2\varepsilon}$	Constant offered by Launder and Spalding (1972)
$C_{3\varepsilon}$	Constant offered by Launder and Spalding (1972)
C_μ	Constant offered by Launder and Spalding (1972)
C^*	Model coefficient for present study for relationship between air concentration and flow depth
$D_{aerator}$	Diameter of aerator duct
Fr	Froude number
g	Acceleration of gravity

G_b	Term for generation of turbulence due to buoyancy
G_k	Term for representing the production of turbulence kinetic energy
h_{inlet}	Depth of flow at inlet
h_{ramp}	Depth of flow over ramp or step
H_s	Height of step
k	Turbulence kinetic energy
K	Dimensionless quantity for relationship between β and L_j
K_1	Model coefficient for present study for relationship between β and geometric properties of flow
K_2	Model coefficient for present study for relationship between β and geometric properties of flow
K_3	Model coefficient for present study for relationship between β and geometric properties of flow
L_j	Length of jet
L_r	Length of ramp
$\dot{m}_{qp}$	Mass transfer term from phase q to phase p
p	Pressure
$\overline{p}$	Time averaged pressure
P	Mean pressure

p'	Fluctuating pressure
$\overline{p'}$	Time averaged fluctuating pressure
P_0	Local pressure
P_v	Vapor Pressure
P_N	Cavity subpressure number
q_a	Air entrainment per meter chute width
q_w	Flow discharge per meter chute width
R^2	Coefficient of determination
s_{ij}	Strain rate tensor
S_{ij}	Mean strain rate tensor
S_{α_q}	Mass source used in volume fraction equation
t	Simulation time
t_j	Jet flight time
t_r	Height of ramp
U_0	Average flow velocity
u_i	Velocity (in the direction of i)
$\overline{u_i}$	Time averaged velocity (in the direction of i)
U_i	Mean velocity (in the direction of i)

u_i'	Fluctuating velocity (in the direction of i)
$\overline{u_i'}$	Time averaged fluctuating velocity (in the direction of i)
V_{ramp}	Velocity of flow over ramp or step
x_i	Location of reattachment point in the direction of x
Y_M	Dilatation dissipation term
z_0	Elevation of channel bottom
α	Ramp angle
β	Air entrainment index
δ_{ij}	Kronecker delta
ΔP	Pressure difference between atmospheric air pressure and lower nappe cavity air pressure
ε	Rate of dissipation
θ	Channel slope
μ	Dynamic viscosity of water
ν	Kinematic viscosity of water
ν_T	Eddy viscosity of water
ρ	Density of water
σ	Cavitation index

CHAPTER 1

INTRODUCTION

Dams have been constructed in different ways and for different needs like irrigation, power generation, water consumption, prevent flooding etc. throughout the history of civilizations. Independent of usage purposes and their construction types, their main function is storing the water on a stream. Capacity of dams are decided as per water demand, precipitation and regime of flow on the stream. Rate of precipitation and regime of flow depend on climate which is hard to predict. Due to variability and instability of factors, safety structures should be constructed like spillways. Spillways are important key structures operating in urgent times to prevent collapse of a dam. Their design life times should be identical to that of the whole dam structure and damages due to high speed free surface flows should be eliminated. One of the main damages occurs on a spillway is due to cavitation.

Pinto (1988) explained vaporous cavitation as the changing of liquid phase to vapor phase by decrease of pressure in flow due to high speeds. During this change vapor bubbles occur and at some point these bubbles encounter with higher pressure zones. Loudly imploding cavities in high pressure zones further generates pressure on bed and cause cavitation damages. The pressure up to 1500 MPa magnitude was observed as a result of collapse of cavities in experiments done by Lesleighter (1988). These continuous high pressure collapses removes small particles from surface of the structure and leads to high damages over the structure in time (Kells and Smith, 1991). Some of the real life examples of cavitation damages listed by Kramer (2004) in chronological order can be seen in Table 1.1.

Table 1.1: Cavitation damages on spillways and outlets (Kramer, 2004 and Demiröz and Darama, 1992)

Year	Project	Damage
1935	Madden Dam, Panama Canal Zone	First efforts being made toward studying the cavitation phenomenon after the dam failure
1941	Boulder Dam, Colorado, USA	Cavitation damage during small discharges due to negative spillway curvature
1941-1983	Hoover Dam, Arizona, USA	Initial cavitation damage in 1941, repaired and damaged again in1983
1960	Grand Coulee Dam, USA	Cavitation damage in the outlets due to abrupt change of flow direction
1964	Palisades Dam, Idaho, USA	Cavitation damage downstream of intake gates
1966	Aldea-Davila Dam, Portugal	Cavitation damage in the auxiliary tunnel spillway
1967	Yellowtail Dam, Montana, USA	Cavitation damage through the tunnel spillway lining in to the foundation rock due to a small (3mm) surface irregularity
1967	Turtle Creek Dam, Kansas, USA	Cavitation in the concrete floor downstream of the seal plate
1970	Blue Mesa Dam, Colorado, USA	Cavitation damage in the outlet structure
1970	Clear Creek Dam, Colorado, USA	Cavitation damage of the concrete outlet conduit
1972	Libby Dam, Montana, USA	Cavitation damage at the centre sluice, coincided with prominent cracks across the invert
1976-1989	Keban Dam, Turkey	Cavitation damages at the spillway chute channels
1977	Tarbela Dam, Pakistan	Cavitation damage in the spillway tunnel due to surface irregularities from a remaining wall
1977	Karun Dam, Iran	Cavitation damage in the open channel spillway firstly induced by surface irregularities and due to the high velocities
1982	Stampede Dam, Nevada, USA	Concrete damage in the outlet structure
1983	Glen Canyon Dam, Colorado, USA	Large damage in the tunnel spillway induced by initial cavitation

Estimating the cavitation potential can help to prevent cavitation damages on a structure. Most of the approaches in the literature for predicting cavitation potential of a flow are based on velocity of the flow. Cassidy and Elder (1984) states that a flow with 11 m/s velocity can damage a channel bed with irregularities. Volkart and Rutschmann (1991) take the limit cavitation velocity for proper smooth concrete surface between 22 m/s and 26 m/s. Another cavitation limit was given per operating head by Oskolkov and Semenkov (1979) which states a cavitation risk for exceeding 50 m.-60 m. Another approach is cavitation number (index) which is a special form of Euler Number (Aydın, 2005) given in Equation 1.1. Pinto (1988) states a cavitation risk for σ <0,25.

$$\sigma = \frac{\left(P_0 - P_v\right)}{\rho U_0^2 / 2} \tag{1.1}$$

where; σ is the cavitation number, P_0 is the local pressure including atmospheric pressure, P_v is the vapor pressure, ρ is the density of the fluid and U_0 is the average flow velocity.

Cavitation phenomenon could be avoided by aerating the flow. Pinto (1988) states that aeration is one of the common ways to prevent the cavitation damages and considering time and economical concerns, it is the best solution. Bottom bed aeration increases the air void ratio which makes mixture more compressible and lowers the velocity of pressure waves. Aeration also increases the dissolved oxygen capacity of the water and gives advantage for downstream natural life and fishery (Arantes et al. 2010). To this end spillways designed to carry medium to high discharges, which are under the high risk of cavitation, often use stepped structure to produce aeration zones for the flow. The aeration over the steps is often made possible by chimneys built on the side of the steps that allow air entrainment from one side of the flow. The air entrainment is further made possible by use of deflecting chutes, which are also known as ramps, located just before the steps. The

most common aerator structures over a spillway are given in Figure 1.1 (Cassidy and Elder, 1984). In this study flow over ramp and step structures are simulated.

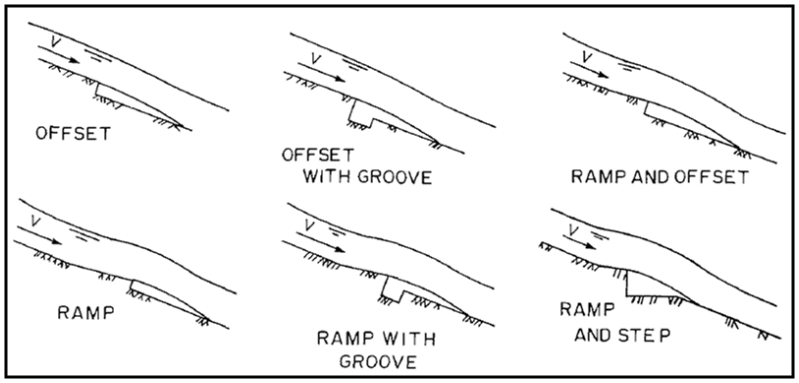

Figure 1.1: Common aerator structures over a spillway (Cassidy and Elder, 1984)

The flow over the ramp and the step could be separated to three major zones. The first zone is the approach zone. This zone is for the flow upstream of step over the spillway, and it ends just before the start of the ramp as shown in the Figure 1.2. This region is immediately followed by a transition zone over the ramp where flow gains upward momentum. Over the step, we can observe the aeration zone where upward trajected nappe flow entrains air both from the upper and the lower interface. The aeration zone ends when flow retouches to the spillway surface. With the re-attachment of the flow the de-aeration zone begins. Air entrainment coefficient, β, can be described as Q_a/Q_w where; Q_a is air discharge on aerators and Q_w is water discharge on spillway.

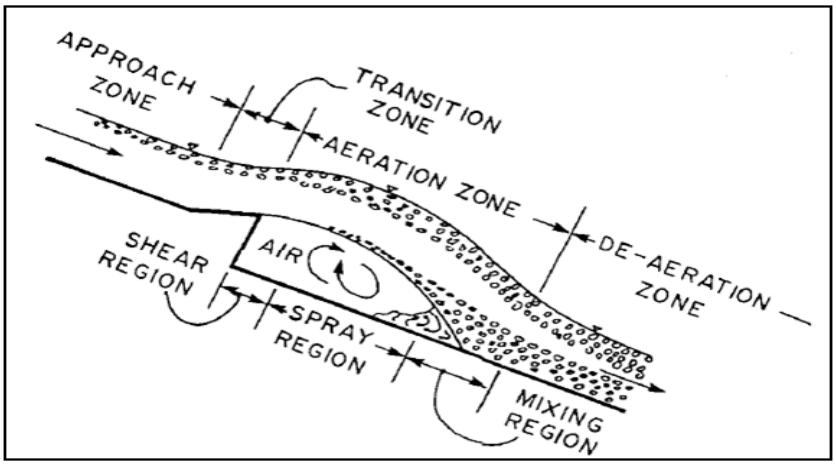

Figure 1.2: The three major zones observed for a nappe flow over a step (Volkart and Rutschmann, 1984)

In this study, average flow features and quantities in the vicinity of spillway aerators are analyzed by numerical methods. For this purposes, 16 cases are analyzed by a commercial CFD software ANSYS Fluent. The main aspect of the study is investigating the effect of ramp angle, flow discharge, aerator size and position over the jet-length, amount of air-entrainment, general flow structure.

In Chapter 2, related experimental and computational studies in literature are briefly summarized. In Chapter 3, computational grid and boundary conditions of current study are explained. Model parameters, governing equations and simulation setup are also part of this chapter. In Chapter 4, results of the analyses are presented. Effect of geometric properties and flow characteristics such as variation of air concentration in streamwise direction and over the flow depth, variation of velocity magnitude after the reattachment point are discussed in detail. At the end of this chapter, a brief summary of results and comparison with previous studies are given. In last chapter, conclusions and future recommendations can be found.

CHAPTER 2

LITERATURE SURVEY

In literature, flows over spillways are commonly studied using physical experiment. Generally, experimental models are used for design of hydraulic structures, however in studies where two fluids with very different properties are going to be in interaction, such as the air entraining water flows, the scale effects become very important. Often the open channel flow studies depend on Froude Similarity. In the case of air entrainment Weber Number becomes important as it represents the surface tension effects. However, it is often difficult to achieve both Weber and Froude similarity in an experimental setting. Due to this, Froude and Euler similitude are essential for modeling and it is commonly observed that small scale ratios gives more realistic results. Due to small scale ratios needed for realistic results, the economy of the experiment is greatly compromised. Lee and Hoopes (1996) indicated scale effects and errors from model observations as one of the reason for cavitation damages. Chanson (1990), studied air demand of the Clyde Dam spillway with a 1:15 scale model, later stated that model studies and prototype results are far from being similar. Due to these limitations, with the advancement in the computational powers, the researchers recently started to prefer numerical modeling of such flows. However, the insight that experimental studies provide could never be denied (Aydın and Öztürk, 2009).

One of the aerator model studies in Turkey was done for multipurpose Keban Dam located on Euphrates River with 17,000 m^3/s flow capacity spillway by Demiröz et al. (1994). Spillways of the Keban Dam were designed and constructed without aerators. After twice operated in flood periods, due to high velocity flows, cavitation damages were observed. For preventing spillways from future damages and

eliminating cavitation risks aerators were recommended. The model was constructed with 1:25 scale and spillway aerators designed according to this model studies. Modifications of spillways were concluded by adding four orifice type aerators on each of them. After construction of aerators prototype pressure differences between the top and bottom of the air jet for different discharges were obtained. These values are used for calculation of analytical air entrainment. In the results of the study, analytical, model and prototype values for air entrainment phenomena are compared. This comparison for the first aerator can be found in Figure 2.1. According to this graph, correction factor for model to prototype value was determined to be around 1.7, which coincides with the recommendation of Volkart and Chervet (1983). Another clear result was the decrease of air entrainment rate by the increase of flow rate.

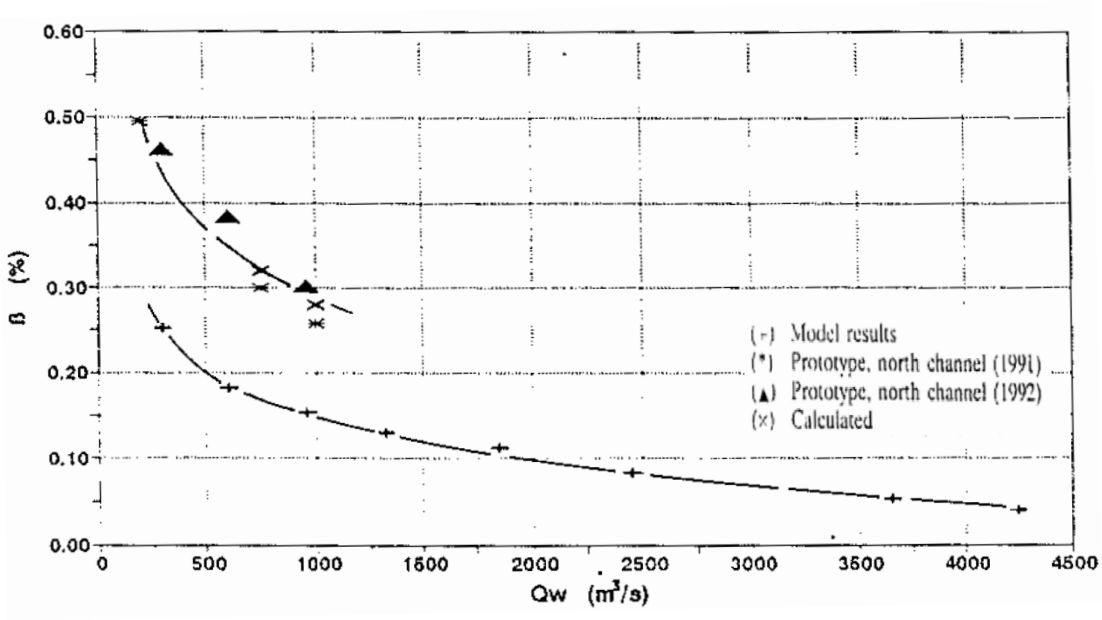

Figure 2.1: Air entrainment comparison (Demiröz et al., 1994)

Another important study on cavitation over a spillway is the study of Deriner Dam by the State Hydraulic Works (DSI) of Republic of Turkey (Kökpınar, 2004). The experimental study focuses on four different discharge values and cavitation indices calculated for these discharges. In the experiments the static pressure at the bottom of

the approach tunnel and the velocity of the flow are measured. Based on their results, they made recommendations on construction and modification of the spillway of Deriner Dam. The recommendations include use of two aerators about 160 m. apart from one another over the spillway.

A similar study by Bhosekar et al. (2012), considers orifice spillway aerators of Subansiri Lower Project of India over the Subansiri River. The experimental part of the study uses 1:25 scaled physical model. Same scale is used in the numerical part of the study. Froude similarity is most conveniently used for free surface flows, however, due to mixture of air and water in the same geometry, geometrical similarity cannot be used as it yields to wrong predictions of Reynolds and Weber numbers. Hence, Weber and Reynolds numbers are limited in a range in order to discard scale effects. The graph of orifice spillway aerator used in the study of Bhosekar et al. (2012) can be seen in Figure 2.2. For numerical model, geometry was created in preprocessor software Gambit and numerical solution was progressed by Fluent. Volume of Fluid (VOF) method was used for describing mixed air-water flow. The k-ε turbulence model was used in the simulations and results are validated by the results from the physical model. Validation plot for air entrainment coefficient, β, can be seen in Figure 2.3. The study shows that air entrainment was related with air entrance area, ramp geometry and Froude number.

Air entrainment ratio is found to be related to some independent variables such as slope of spillway and aerator, heights of the ramp and the offset, flow depth, Froude number and cavity subpressure in a previous study by Rutschmann and Hager (1990). In conclusion, air entrainment was linked to Euler number directly in this study.

In literature, there are studies that involve best of both experimental and numerical investigation of these flows. In the study of Arantes et al. (2010), experimental and computational methods are employed concomitantly. As a result, it was found that calibrated numerical models can be used for determination of bottom inlet spillway aerators.

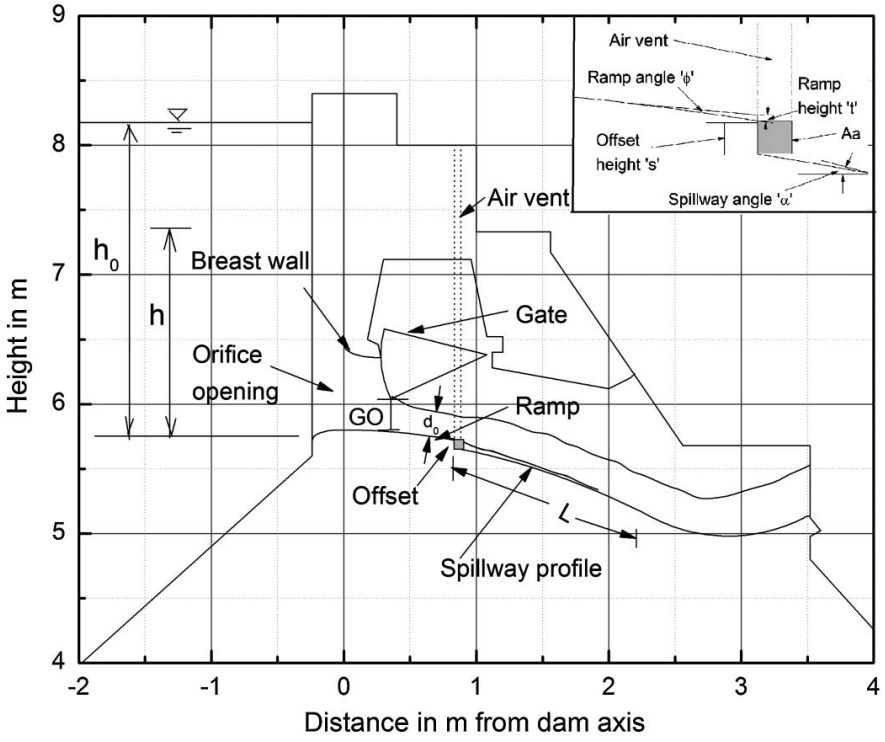

Figure 2.2: Orifice spillway aerator sketch (Bhosekar et al., 2012)

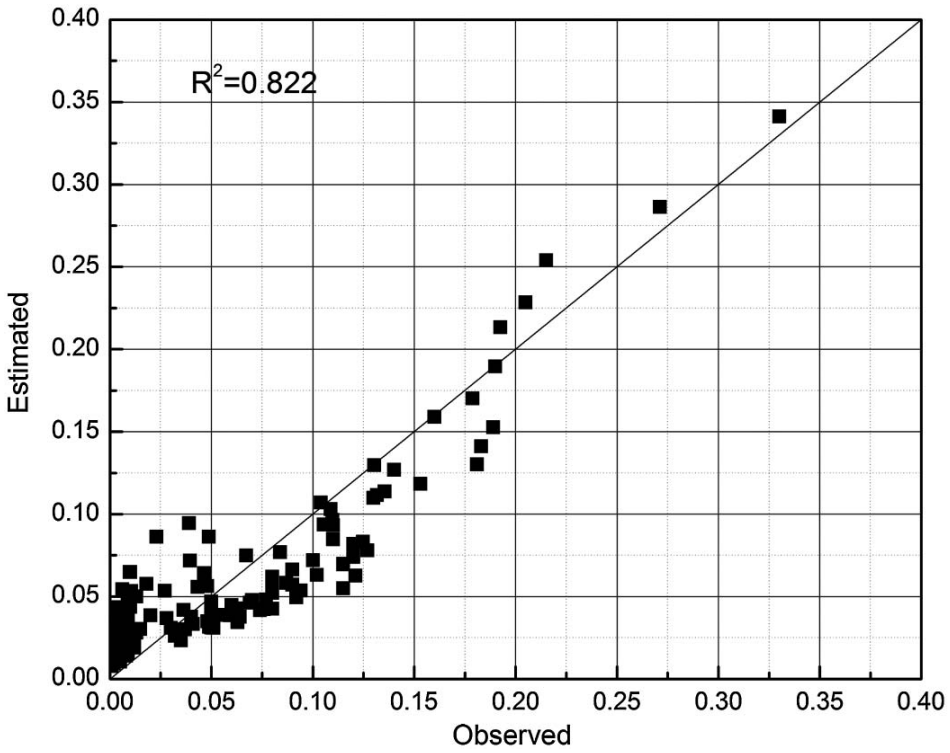

Figure 2.3: Plot of β observed vs. estimated (Bhosekar et al., 2012)

Jet-length is a common parameter used for explaining air entrainment in spillway flows. Most of the empirical equations use jet-length for determining the air entrainment ratio. The first study that offers such an empirical equation for jet-length is of Schwartz and Nutt (1963). Likewise, Pan et al. (1980) and Pinto et al. (1982) showed a relation between geometry of jet-length and air entrainment. In the study of Kökpınar and Göğüş (2002), the major forces in an open channel flow is listed as inertial, gravitational and pressure forces. Viscous and surface pressure forces, which are defined by Reynolds and Weber numbers, were eliminated for air entrainment in open channel problems. Air entrainment ratio is given as a function of aerator and chute channel geometry and flow characteristics. Froude number, slope of chute channel, height of deflector, aerator geometry terms are defined as independent variables and air entrainment ratio, jet-length, dimensionless pressure number are defined as dependent variables. Experiments took place at Middle East Technical University (METU) in a 5.0 m long and 0.1 m wide Plexiglass flume. Different channel slopes, ramp angles, heights and lengths are considered in the study, and there is also a constant step as part of the experimental setup. Sketch of the experimental setup and the geometric parameters considered in the study of Kökpınar and Göğüş (2002) can be seen in Figure 2.4 and Table 2.1, respectively. Observations show that aeration starts at free surface and after the jump both lower and upper surfaces are aerated until the jump is over. Study offers an empirical formula in the light of observations, which summarizes the relation between the jet-length and all the other parameters affecting air entrainment case, performance and efficiency of an aerator.

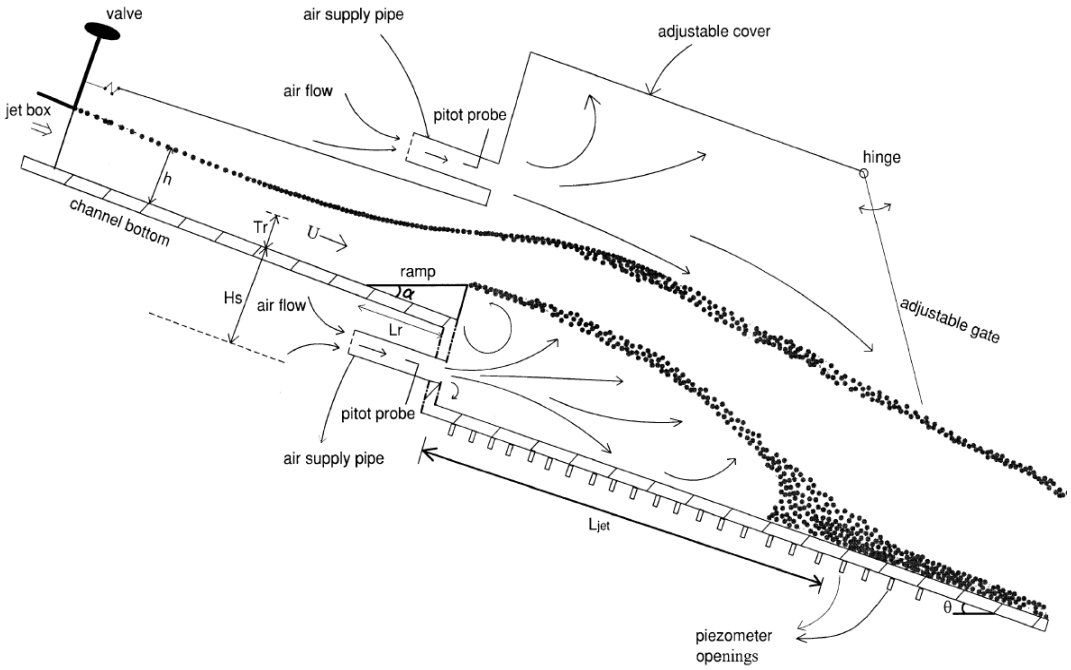

Figure 2.4: Experimental setup (Kökpınar and Göğüş, 2002)

Table 2.1: Aerator geometries (Kökpınar and Göğüş, 2002)

Channel Slope tanθ	**Ramp Angle** α (°)	**Ramp Height** t_r (m)	**Ramp Length** L_r (m)	**Step Height** H_s (m)
0	0	0	0	0.05
0	5.71	0.005	0.05	0.05
0	5.71	0.010	0.10	0.05
0	5.71	0.020	0.20	0.05
0.17	0	0	0	0.05
0.17	5.71	0.005	0.05	0.05
0.17	5.71	0.010	0.10	0.05
0.17	5.71	0.020	0.20	0.05
0.57	0	0	0	0.05
0.57	5.71	0.005	0.05	0.05
0.57	5.71	0.010	0.10	0.05
0.57	5.71	0.020	0.20	0.05

In the study of Tan (1984) which is similar to the study of Rutschmann and Hager (1990), jet-length was based on subpressure number, P_N, which is a function of atmospheric and lower nappe cavity pressure and gravitational forces. The validation of the study was done based on the study of Schwartz and Nutt (1963).

Different from air entrainment ratio and jet-length studies, there are studies on aerator spacing on a spillway in order to maintain continuous aeration. According to the model studies of Lesleighter and Chang (1981) the distance between aerators should be 40 m, while Pinto et al. (1982) suggests that an aerator should be able to protect a distance of 50-100 m over a spillway, in some applications they found that using many aerators back to back on a spillway may lead to over aeration, which is also an undesirable condition. Kells and Smith (1991) propose limits for maximum air concentration of 45% and minimum of 8% for the proper protection of the spillway structure from cavitation. The recommended spacing between the aerators is based both on maximum and minimum air concentration and on the required decay rate of air concentration of 0.4-0.8% per meter length of the spillway. Based on their results, in order to satisfy above conditions, they propose a minimum spacing of 23.1 m and maximum spacing of 92.5 m.

Two different air concentration profiles can be seen in Figure 2.5 from the study of Volkart and Rutschmann (1984). This figure shows air concentration values for two different water discharges. The air concentration diminishes quickly after the impact zone over the streamwise direction in short distance of 15 m in their model study. In the study, the air distribution was mentioned to depend on distance to sidewall and local Froude number. However, study does not suggest any further standards in terms of sidewall effects and bottom aeration via consecutive aerators.

In a more recent study of Kramer et al. (2006) a physical model with 14 m long and 0.50 m wide channel was constructed to investigate longitudinal aerator spacings over hydraulic chutes with variable bottom slopes. Air concentration readings were taken along the model with fiber-optical probes. The schematics of the physical model can be seen in Figure 2.6. The readings were used for plotting air contours in

longitudinal direction of the spillway and enables identification of location of critical point where next aerator could be placed.

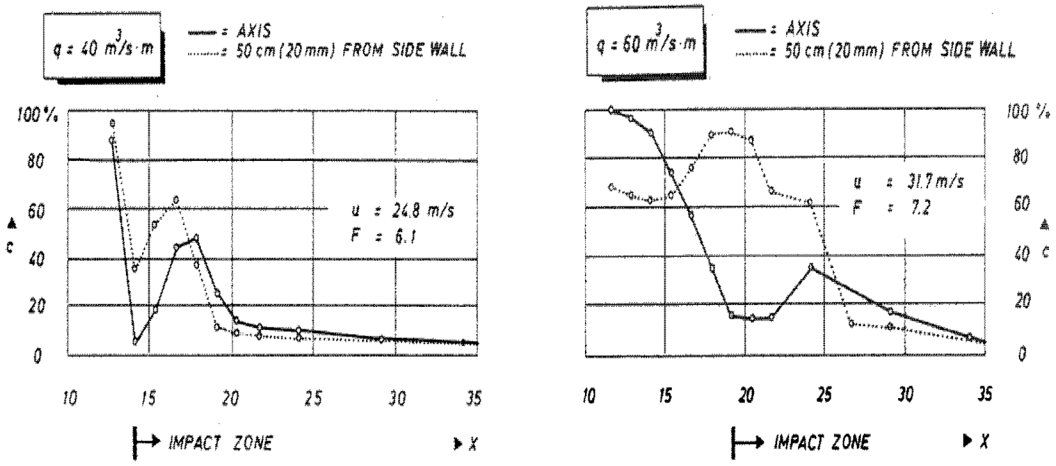

Figure 2.5: Air concentration profiles along channel bottom, 10 cm above the bottom. (Volkart and Rutschmann, 1984)

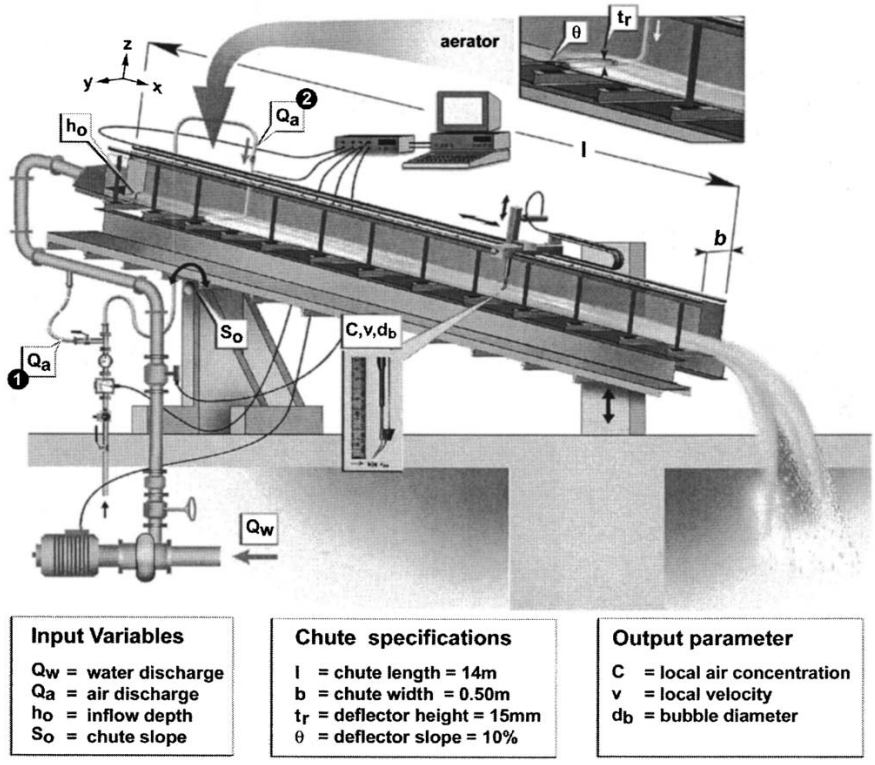

Figure 2.6: Physical model (Kramer et al., 2006)

In the recent numerical study of Aydın and Öztürk (2009), a commercial CFD software is used for numerical simulation of flow over a stepped spillway with Algebraic Slip Mixture (ASM) method and k-ε model. Numerical verification of model is done according to ASME (American Society of Mechanical Engineers) statements. Geometry of the model was based on the prototype geometry of previous studies done by Demiröz (1985). Demiröz used 1:25 length scale and Froude similarity in experimental model. In the study of Demiröz; air entrainment, jet-length and lower nappe pressures are observed for different channel slopes, ramp angles and ramp heights. As a conclusion these parameters affects jet-length and air entrainment. Aydın and Öztürk also emphasized the fact that aeration increases compressibility of the mixture and lowering the velocity of pressure waves. The geometric model of the studies of Aydın and Öztürk (2009) and aerator geometries of the study of Demiröz (1985) can be seen in Figure 2.7 and Table 2.2, respectively.

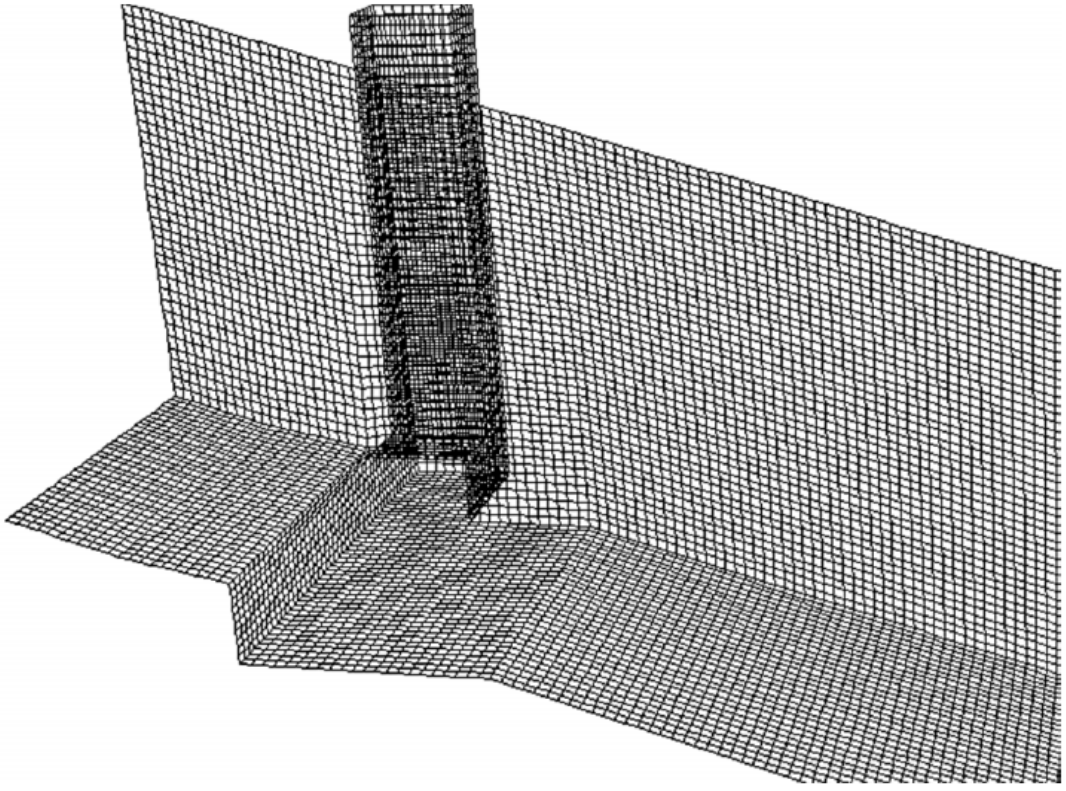

Figure 2.7: Geometric model (Aydın and Öztürk, 2009)

Table 2.2: Aerator geometries (Demiröz, 1985)

Channel Slope tanθ	**Ramp Angle** α (°)	**Ramp Height** t_r (m)	**Ramp Length** L_r (m)
0.30	1.90	0.002	0.06
0.30	3.77	0.004	0.06
0.30	5.71	0.006	0.06
0.30	7.59	0.008	0.06
0.30	9.45	0.010	0.06
0.60	0.95	0.001	0.06
0.60	1.90	0.002	0.06
0.60	2.86	0.003	0.06
0.60	3.81	0.004	0.06
1.25	1.90	0.002	0.06
1.25	3.77	0.004	0.06
1.25	5.71	0.006	0.06
1.25	7.59	0.008	0.06
1.25	9.45	0.010	0.06

The major advantage of numerical models over physical ones is the economy while eliminating the scale effects. In this study, different from the study of Aydın and Öztürk (2009), Volume of Fluid (VOF) method is used for free surface tracking. Aeration of flow is made possible by using circular cross sectioned bottom aerators. The size of the aerators, the height of the deflector, locations of the aerators over the step and the discharge of the flow are considered as the variables in the study. The numerical simulations are conducted to investigate the effect of each of these parameters on the air entrainment. The numerical results of this study are compared to the results obtained from the empirical formulas of previous studies.

CHAPTER 3

COMPUTATIONAL GRIDS, MODEL PARAMETERS AND SIMULATION SETUP

3.1 Computational Grid and Boundary Conditions

General geometry of the computational domain in this study is based on the previous studies of Demiröz (1985) and Aydın (2005). This is in order to assess the effects of variables and for validation of the results. The simulation domain is a 21.5~36.5 m long open-channel with bottom slope of 0.3 (θ=16.70°). The channel has rectangular cross section. The width of the channel is 5 m. In some of the simulations, 1.5 m-long ramp is attached to the domain just before the step in order to deflect the flow in the vertical direction. In this study, different from the previous studies, a 1 m-high step is located 5 m downstream of the inlet and the aerators with circular cross-sections are placed on the horizontal surface of the step. The plan and the side view of the computational grid can be seen in Figure 3.1 and Figure 3.2, respectively.

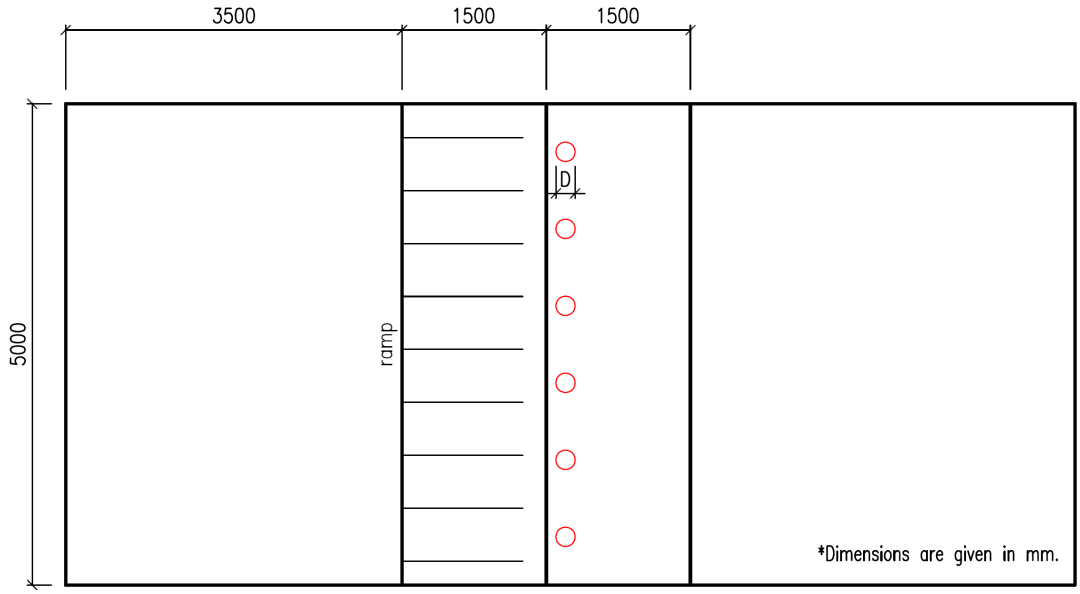

Figure 3.1: Plan view of the computational grid with a deflector

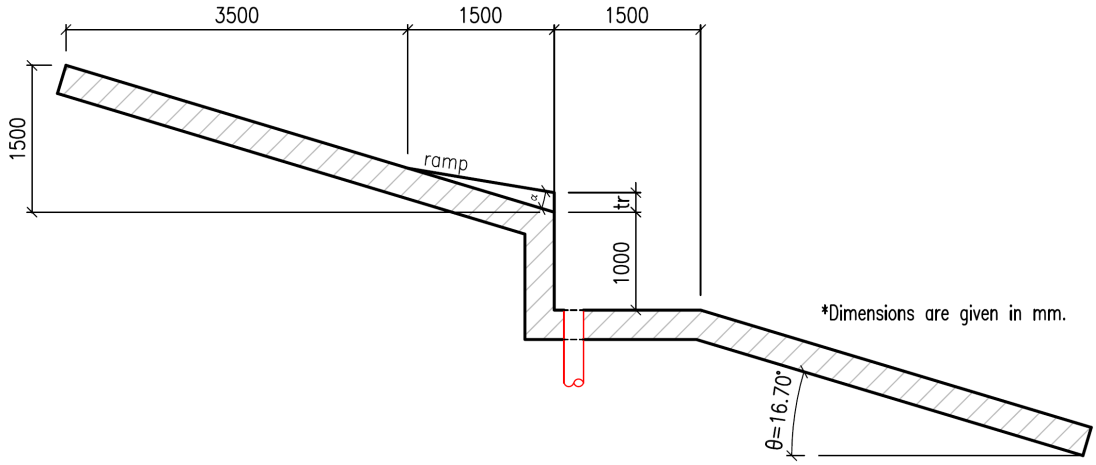

Figure 3.2: Side view of the computational grid with a deflector

The computational grids for the simulations are created by the preprocessing software Gambit. The view of the mesh near the aerators is given in Figure 3.3. Total number of cells in the computational grids are nearly 1.8 million. Grids are made out of hexahedral elements. The mesh is denser in the regions where water flow is

expected. In the computational grid where the fluid phase is air, which represents the region above the flow, larger cell sizes are used for the economical reasons. The average cell size is taken as (ΔX, ΔY, ΔZ)=(0.1, 0.05, 0.1) in meters. This average cell size is found to be small enough for the accuracy of the turbulence model, as suggested by Ansys Fluent.

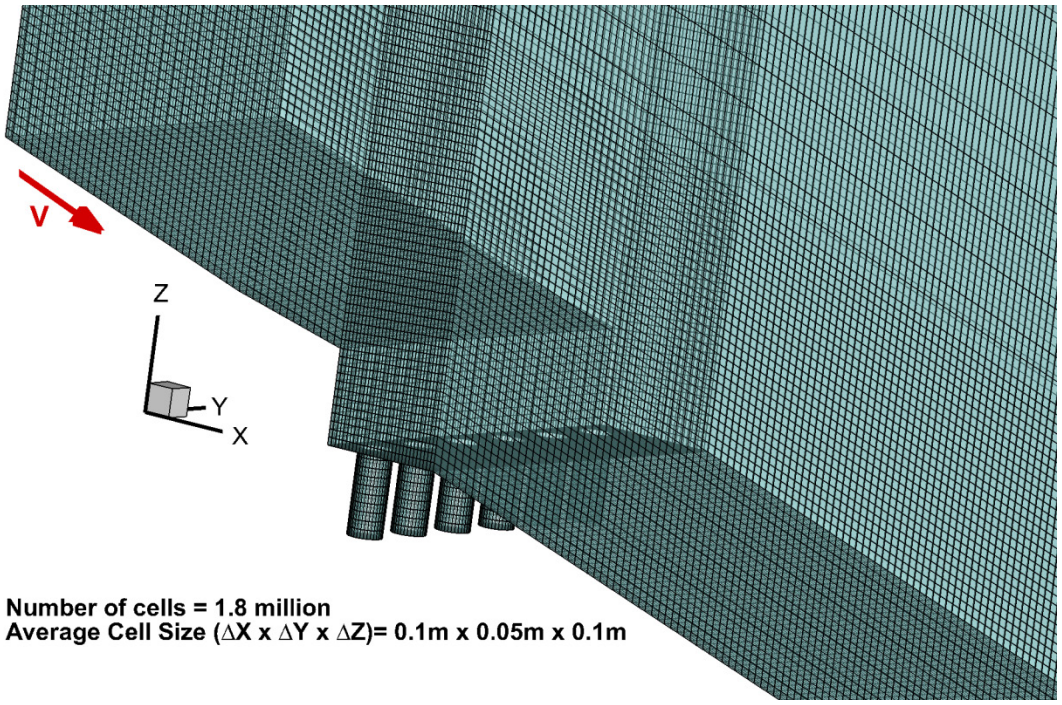

Figure 3.3: View of computational grid near the aerators

The inlet is treated as mass flow inlet, variable inlet heights are determined for this boundary due to changing velocities and discharges of flow. The top boundary, the boundary above the inflow and the aerator pipes are taken as pressure inlets and the outflow is treated as pressure outlet as given in Figure 3.4. For the pressure inlet and outlets, the pressure values are defined as atmospheric pressure. These boundaries could work both as inlets and outlets for the air phase. The sides and the bottom of the domain are treated as no-slip smooth walls.

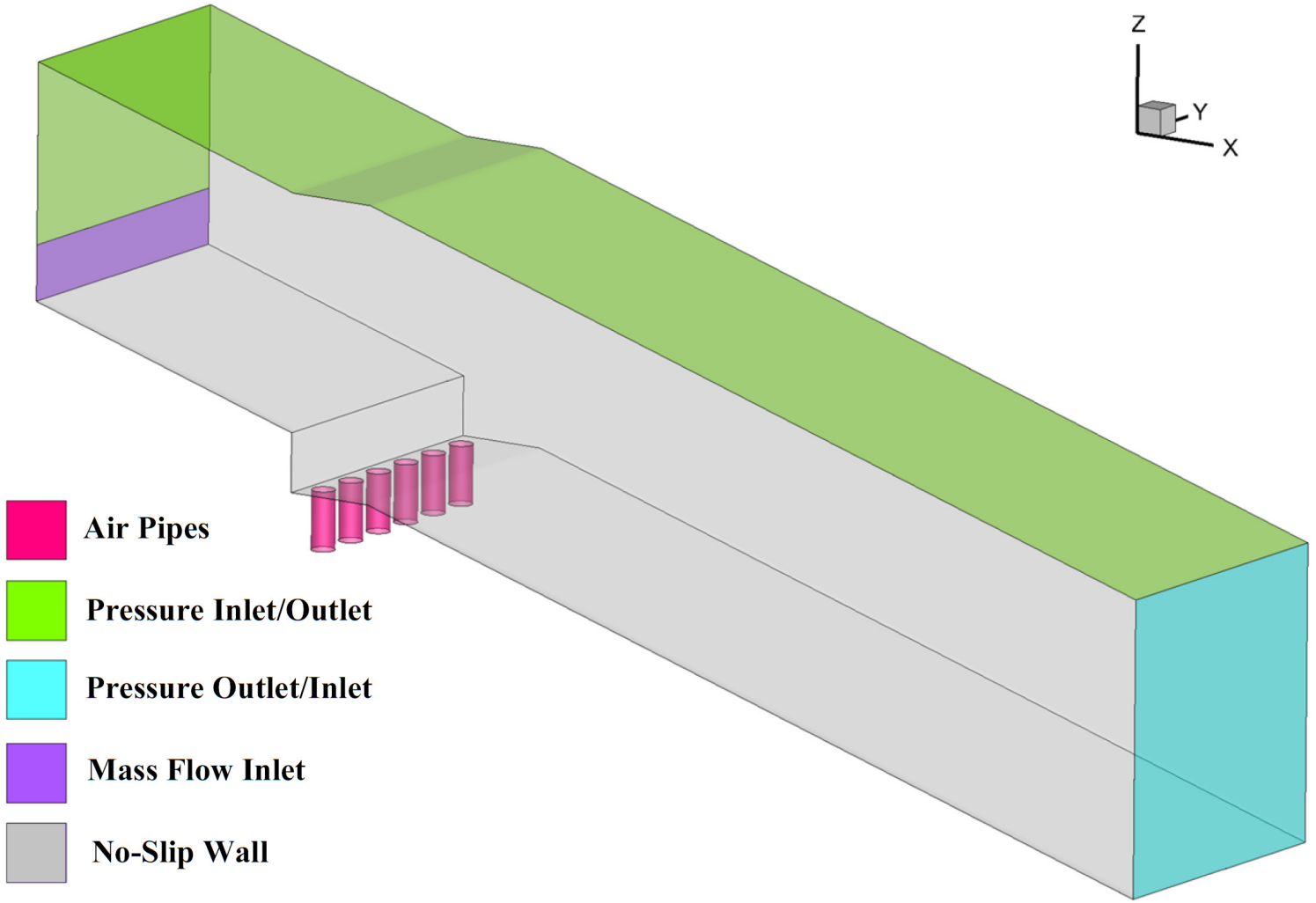

Figure 3.4: Boundary conditions

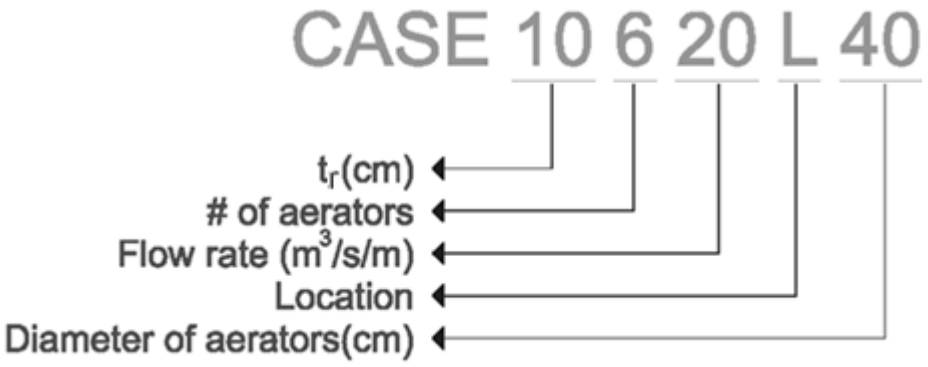

Figure 3.5: The naming of each simulation case in this study

The Figure 3.5 is related to the naming of the cases. The name of each case is given such that first two digits show the height of the ramp in centimeters, the next digit is for the number of aerators that is used in the simulations, following two digits show the unit discharge in m^3/s/m, the letter L in the name of the case is for linear positioning of the aerators on the step, while the letter S is for the scattered positioning of the aerators and the letter F is for far positioning. The final digits in the name is for the diameter of the aerators in centimeters. The linear, scattered and far placement of the aerators with respect to one another are shown in Figure 3.6. Some simulations have extra indicators in parentheses at the end of their names such as the inflow Froude number. Four different diameters for aerators are considered. These are 20, 40, 49 and 57cm. Three different discharge values are simulated (20, 40 and 70 m^3/s/m) which are identical to the ones used in the studies of Demiröz (1985) and Aydın (2005). The flow depths at the inlet boundary are also taken from these studies for the initialization of the simulations. However, in order to observe the effect of Froude number on aeration and flow characteristics several variations of CASE10640L40 are simulated using different initial flow depths. Effect of ramp height is tested by simulating cases with no ramp, and with ramp of height, t_r, 10 cm with α=3.56° and 20 cm with α=7.23°. Finally, the effect of number of aerators is investigated using total of 3, 4 and 6 aerators in three different simulations. In these three simulations, total cross sectional area of the aerators are equal. The effect of position of aerators is considered in simulations with linear, scattered and far

positioning. In the linear positioning the aerators are placed over a straight line, the nearest point of the aerators are about 10 cm away from the vertical drop of the step. In the scattered cases, the aerators are placed in two rows, the distance between these two rows is about 10 cm for 20 cm- diameter aerators and 40 cm for 40 cm-diameter aerators (please see Figure 3.6). In the far positioning, one of the rows of scattered case is further moved to the end of the step. It is placed 10 cm before the end of the step. The cases are listed in Table 3.1. Total of 16 simulations are conducted for the study.

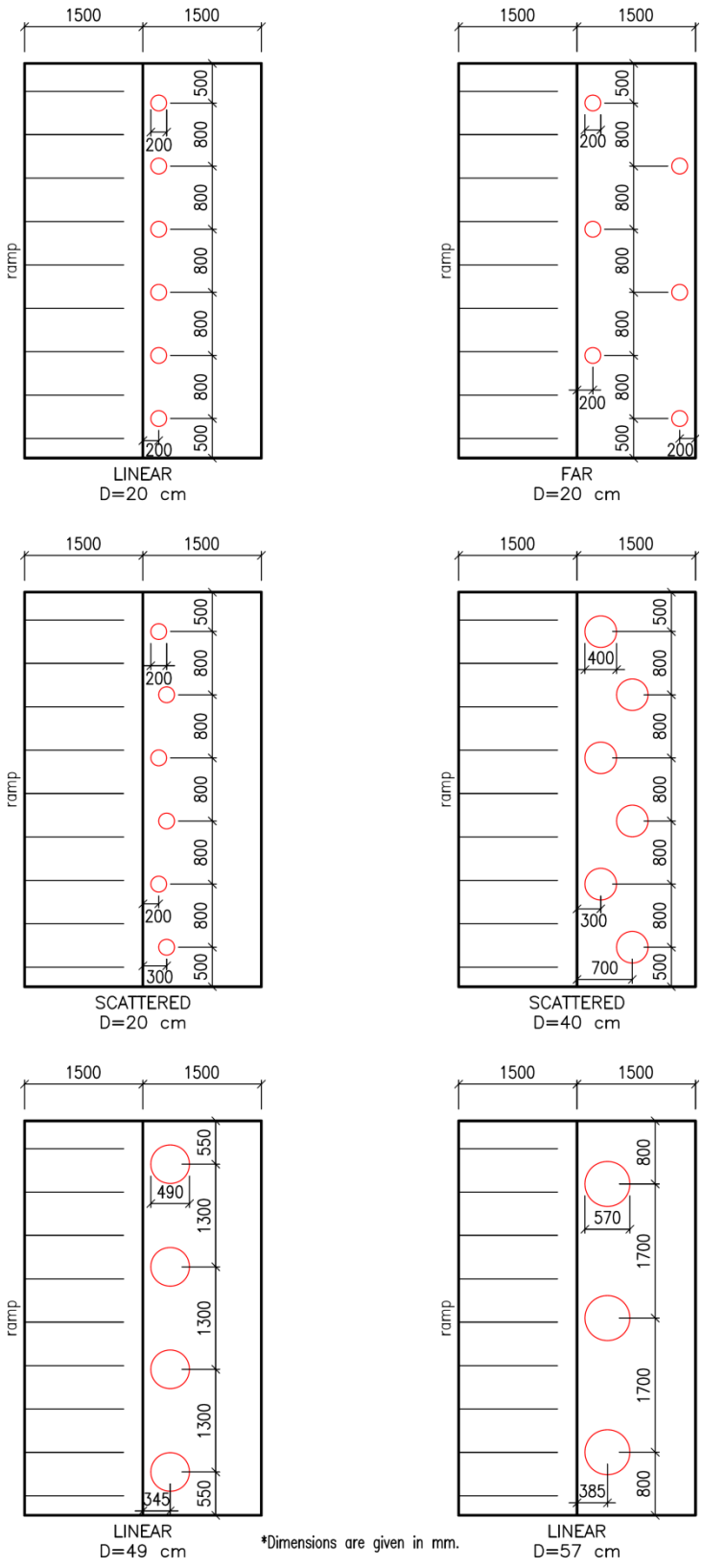

Figure 3.6: Locations for aerators

Table 3.1: Simulation matrix

Case	t_r (cm)	# of aerator	q_w ($m^3/s/m$)	Location	$D_{aerator}$ (m)	h_{inlet} (m)
00620L20	0	6	20	LINEAR	0.2	0.94
00620S20	0	6	20	SCATTERED	0.2	0.94
00620F20	0	6	20	FAR	0.2	0.94
00620L40	0	6	20	LINEAR	0.4	0.94
00620S40	0	6	20	SCATTERED	0.4	0.94
10620L20	10	6	20	LINEAR	0.2	0.94
10620L40	10	6	20	LINEAR	0.4	0.94
10440L49	10	4	40	LINEAR	0.4	1.65
10340L57	10	3	40	LINEAR	0.4	1.65
10640L40(120)	10	6	40	LINEAR	0.4	1.20
10640L40(140)	10	6	40	LINEAR	0.4	1.40
10640L40	10	6	40	LINEAR	0.4	1.65
10640L40(200)	10	6	40	LINEAR	0.4	2.00
10640L40(250)	10	6	40	LINEAR	0.4	2.50
10670L40	10	6	70	LINEAR	0.4	2.70
20620L40	20	6	20	LINEAR	0.4	0.94

3.2 Model Parameters

In this study, high velocity flows are investigated in the vicinity of the aerators. This means simulated flows have large Reynolds numbers (55-135x10^6) where Reynolds number is a function of average velocity, hydraulic radius and kinematic viscosity of the fluid. The flow is aerated; therefore, it is a two-phase flow that consists of incompressible fluid water and compressible fluid air. These types of flows get quite complex with the mixing of these two phases with the effect of turbulence. The challenge is to account for all these conditions in the numerical models as much as possible.

3.2.1 Governing Equations

According to Markatos (1986) and many other researchers, understanding the nature of turbulent flow and expressing it mathematically is a difficult task. Navier-Stokes momentum-transport equations are considered as the most sufficient way to described turbulent flows. Tennekes and Lumley (1972), described turbulence as flow feature instead of fluid (gas or liquid) feature. It depends on Reynolds number. Turbulence does not depend on atomic characteristics of the liquid, generally its nature is same for all liquids. The dominant character of the turbulent flow is its irregularity, which causes it to be very complex. This irregularity is three-dimensional and also rotational. The flow is also diffusive and dissipative. This means flow has a tendency for mixing and viscous shear stresses increase internal energy of the flow, which in return increases the momentum rates.

$$\frac{\partial \rho}{\partial t} + \frac{\partial}{\partial x_i}\left(\rho u_i\right) = 0 \tag{3.1}$$

$$\rho \frac{\partial u_i}{\partial t} + \frac{\partial \rho u_i u_j}{\partial x_j} = -\frac{\partial p}{\partial x_i} + \frac{\partial}{\partial x_j}(2\mu s_{ij}) \tag{3.2}$$

General form of conservation of mass formulation is given in Equation 3.1 and conservation of momentum is described in Equation 3.2, where s_{ij} is the strain-rate tensor given in Equation 3.3 and μ is the dynamic viscosity of the fluid.

$$s_{ij} = \frac{1}{2}\left(\frac{\partial u_i}{\partial x_j} + \frac{\partial u_j}{\partial x_i}\right) \tag{3.3}$$

Instead of solving these equations for all values of time and space, a simplified form can be used. The simplified form of these equations are named as Reynolds-Averaged Navier-Stokes (RANS) equations. Time averaged values are used in this method and the main point is writing field variables in two parts, which are mean and fluctuating parts given in Equation 3.4 and Equation 3.5 where capital terms are for mean and terms with apostrophe (') are for fluctuating parts.

$$u_i = U_i + u_i' \tag{3.4}$$

$$p = P + p' \tag{3.5}$$

Equation 3.4 and Equation 3.5 should satisfy below conditions;

$$\overline{u_i} = U_i \quad , \quad \overline{u_i'} = 0 \tag{3.6}$$

$$\overline{p} = P \quad , \quad \overline{p'} = 0 \tag{3.7}$$

Here, the bar ($\overline{\ }$) above the variable shows the time averaging. RANS equations for incompressible fluids are given below (Nguyen, 2005).

$$\frac{\partial U_i}{\partial x_i} = 0 \tag{3.8}$$

$$\rho \frac{\partial U_i}{\partial t} + \rho \frac{\partial}{\partial x_j}\left(U_i U_j\right) = -\frac{\partial p}{\partial x_i} + \frac{\partial}{\partial x_j}(2\mu S_{ij} - \rho \overline{u_i' u_j'}) \tag{3.9}$$

The mean strain-rate tensor S_{ij} given in Equation 3.10.

$$S_{ij} = \frac{1}{2}\left(\frac{\partial U_i}{\partial x_j} + \frac{\partial U_j}{\partial x_i}\right) \tag{3.10}$$

By combining these expressions and eliminating density, ρ from the equations above final expression for RANS equations is obtained as given in Equation 3.11.

$$\frac{\partial U_i}{\partial t} + U_j \frac{\partial U_i}{\partial x_j} = -\frac{\partial p}{\partial x_i} + \nu \frac{\partial^2 U_i}{\partial x_i \partial x_j} - \frac{\partial \overline{u_i' u_j'}}{\partial x_j} \tag{3.11}$$

3.2.1 k- ε Model

The final form of the RANS equations cannot be solved without extra equations due to Reynolds stresses ($\overline{u'_i u'_j}$), which are related to the turbulence. This is also referred as 'closure' problem. These Reynolds stresses are fixed with closure models by using kinetic eddy viscosity (ν_T) hypothesis and one of them is Boussinesq approximation where ν_T is assumed as an isotropic scalar quantity.

$$-\overline{u_i' u_j'} = 2\nu_T S_{ij} - \frac{2}{3} k \delta_{ij} \tag{3.12}$$

where δ_{ij} is the Kronecker delta and k is the turbulent kinetic energy.

$$k = \frac{1}{2}\overline{u_i' u_j'} \tag{3.13}$$

The standard k-ε Model is one of the turbulence models available in Ansys Fluent (Ansys, 2011). This model was first proposed by Launder and Spalding in 1972 and become popular in engineering flow calculations. The model can be used for determining turbulent length and time scale.

The model includes two transport equations, turbulent kinetic energy (k) and its rate of dissipation (ε). Kinetic energy term (k) can be expressed using the fluctuating part of the velocity in turbulent flows. The transport equation of k could be obtained by mathematically manipulating the Navier-Stokes equations using Reynolds-averaging. However, expressing dissipation rate (ε) is not that simple. This term is introduced using physical reasoning in order to conclude the model. This model can only be used for fully turbulent flows. Turbulence kinetic energy and rate of dissipation formulations are given in Equation 3.14 and 3.15, respectively.

$$\frac{\partial}{\partial t}(\rho k) + \frac{\partial}{\partial x_i}(\rho k u_i) = \frac{\partial}{\partial x_j}\left[\left(\mu + \frac{\mu_t}{\sigma_k}\right)\frac{\partial_k}{\partial x_j}\right] + G_k + G_b - \rho\varepsilon - Y_M \tag{3.14}$$

$$\frac{\partial}{\partial t}(\rho\varepsilon)+\frac{\partial}{\partial x_i}(\rho\varepsilon u_i)=\frac{\partial}{\partial x_j}\left[\left(\mu+\frac{\mu_t}{\sigma_\varepsilon}\right)\frac{\partial_\varepsilon}{\partial x_j}\right]+C_{1\varepsilon}\frac{\varepsilon}{k}(G_k+C_{3\varepsilon}G_b)-C_{2\varepsilon}\rho\frac{\varepsilon^2}{k} \quad (3.15)$$

$$\mu_t=\rho C_\mu\frac{k^2}{\varepsilon} \quad (3.16)$$

In these equations, G_k term is related with generation of turbulent kinetic energy according to velocity gradients of mean velocities. G_b is the term related with buoyancy affects. Y_M covers the role of fluctuating dilatation over the total dissipation rate. $C_{1\varepsilon}$, $C_{2\varepsilon}$, $C_{3\varepsilon}$ and C_μ are constants offered by Launder and Spalding (1972).

3.2.2 VOF Model

The VOF (Volume of Fluid) model is basically used for free surface modeling by using volume fraction equations. General form of this model can be used for limitless number of fluids where these fluids also take part in the same set of momentum equations. This method is suitable for white water flows and give possibility for observing steady and transient flow consist of liquid and gas.

Ansys Fluent allows use of VOF model with some limitations. The domain should be filled with fluids defined at the beginning and only one of them can be compressible gas. All fluids share same set of equations. In the simulations, water and air are selected as two phases that are in interaction. Volume fraction of water in a cell is defined as α_w. In a cell inside the computational grid the value of α_w could be 0 , if there is no water in the cell. This indicates that the cell is filled with air phase. If the value is equal to 1, then this shows that the cell is completely occupied by water, and if the value is between 0 and 1 in other words, $0< \alpha_w <1$, then both phases exist in this cell in some ratio (Ansys, 2011).

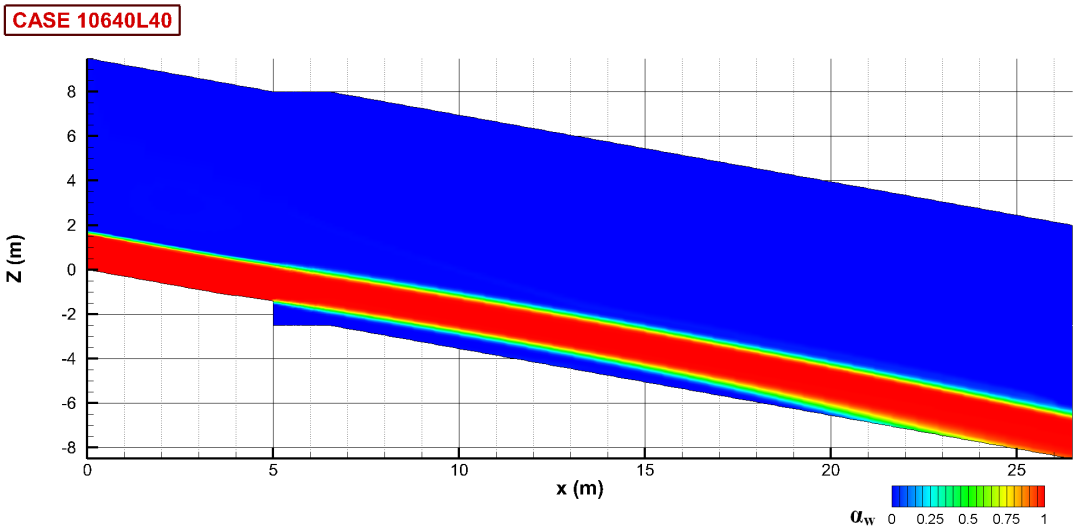

Figure 3.7: Volume fraction of water for Case10640L40

Figure 3.7 represents volume fraction of water for Case10640L40. In this study as the simulations only consider two phases, namely air and water, the volume fraction of air in a cell could simply be expressed as (1-α_w). By solving the volume fraction of the phases with the continuity equation, tracking of the interface between the phases could be accomplished. The general equation for volume fraction is given below (Ansys, 2011).

$$\frac{1}{\rho_q}\left[\frac{\partial}{\partial t}\left(\alpha_q\rho_q\right)+\nabla\cdot\left(\alpha_q\rho_q\vec{v_q}\right)=S_{\alpha_q}+\sum_{p=1}^{n}\left(\dot{m}_{pq}-\dot{m}_{qp}\right)\right] \tag{3.17}$$

Here, $\dot{m}_{qp}$ is the mass transfer from phase q to phase p and $\dot{m}_{pq}$ is the mass transfer from phase p to phase q. S_{α_q} is the mass source. There is no mass transfer between phases in the simulations and additional mass source does not exist. Due to this the right-hand side of the equation is equal to zero.

3.3 Simulation Setup

The simulations are carried using Ansys Fluent, which is the one of the most common CFD software used for analyzing three dimensional (3D) flows. The

launcher offers the options given in Figure 3.8 at the start of the software. In this study, the flow domain is three dimensional, simulations are done using double precision solver and depending on the machine capabilities the parallel processing option could be employed as shown in the figure.

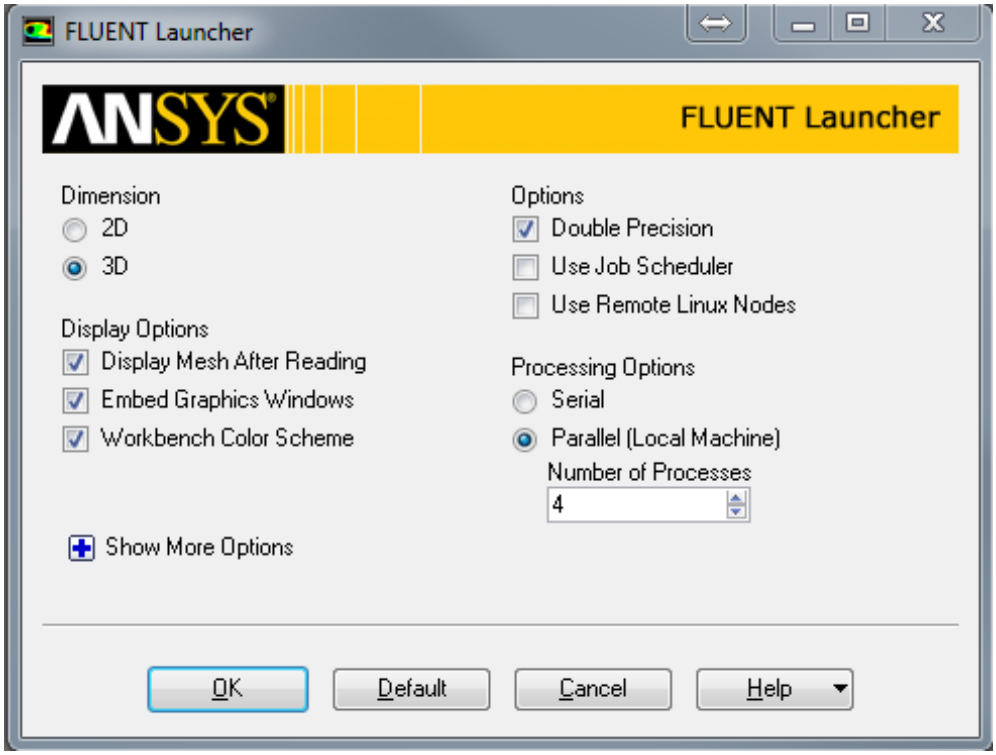

Figure 3.8: User interface of Ansys Fluent launcher

Geometry and boundary conditions are imported to the software after launching the program. The modeling fluid for the flow is selected as water with density of 998.2 kg/m^3 and dynamic viscosity of 0.001003 Pa.s. Initially the domain is assumed to be filled with air. Air is determined as the first phase and water as second phase. In software, the fluid with smaller density should be defined as first phase for computational stability reasons. In the simulations, gravitational acceleration is also taken into account as expected for the open channel flows. Standard k-ε model is used in the runs. Some of these selections can be seen in Figure 3.9.

Pressure based solver is selected in order to employ multiphase VOF model in the study. In this method pressure equations are used for satisfying mass conservation of velocity field. The atmospheric pressure is defined near the topmost boundary. In the solution methods PISO Scheme is selected as pressure-velocity coupling. Spatial discretization options are chosen as PRESTO for pressure, first order upwind for momentum, second order upwind for volume fraction and first order upwind for turbulent kinetic energy and turbulent dissipation rate. First order implicit transient formulation is used for time marching.

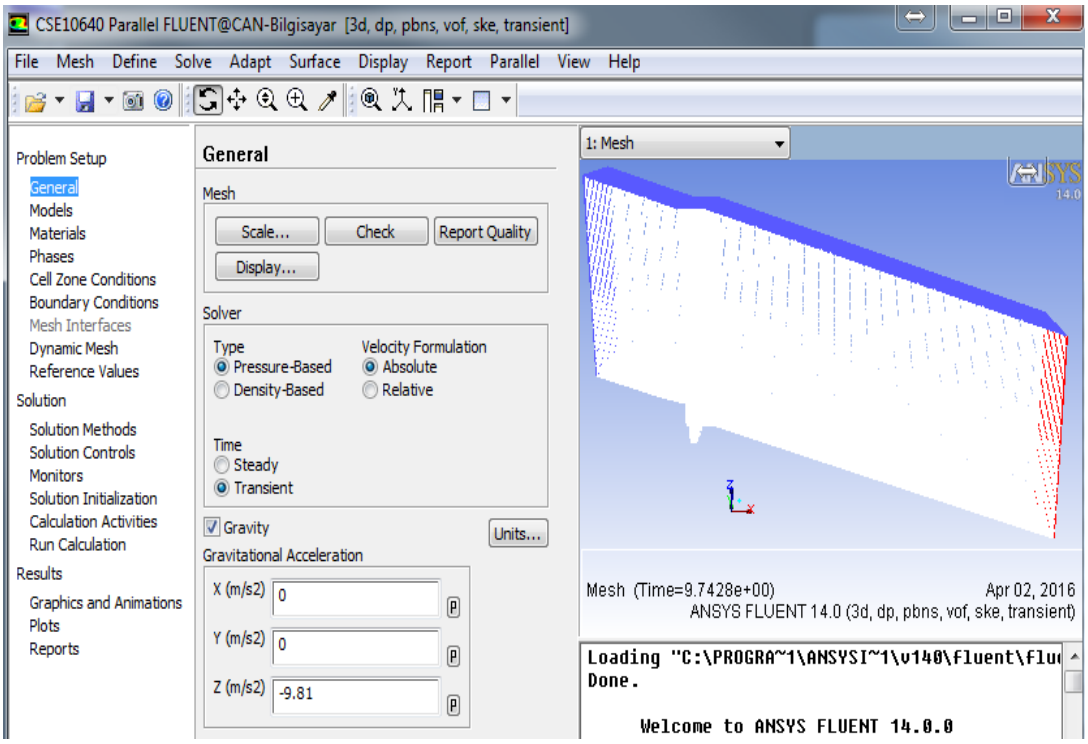

Figure 3.9: User interface of Ansys Fluent - General view

The unsteady simulations run with fixed time step Δt of 0.01 s (please see Figure 3.10). Maximum 20 inner iterations are done per time step. Number of time steps is taken as 1000, which means the total simulation time is 10 s. The flow-through time, in other words, the time for one fluid particle to move from inlet to outlet of the

domain nearly takes 1 s in average in all the simulations where the average velocity of the flow is generally above 20 m/s and the domain length is about 20-30 m. Therefore, all the simulations are carried out for approximately 10 flow-through times. This duration is observed to be enough for flow to reach steady-state. One run with total simulation time of 10 s takes approximately 5 days with the Intel Core i7-2670QM CPU (4 Cores) and 8GB memory laptop computer.

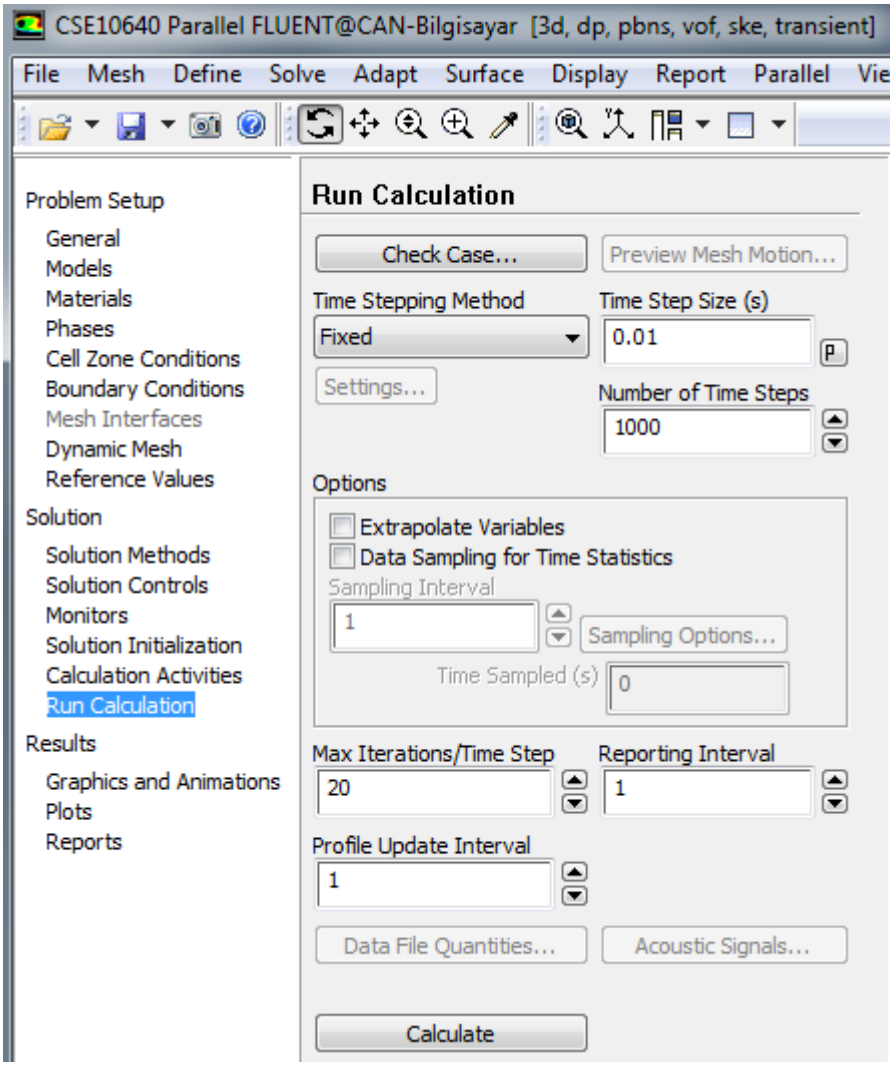

Figure 3.10: User interface of Ansys Fluent – Run calculations tab

CHAPTER 4

RESULTS AND DISCUSSION

4.1 Introduction

In this section the results from the simulations are presented and discussed. The comparisons between the cases are presented. The common features of all the simulations are summarized in this sub-section.

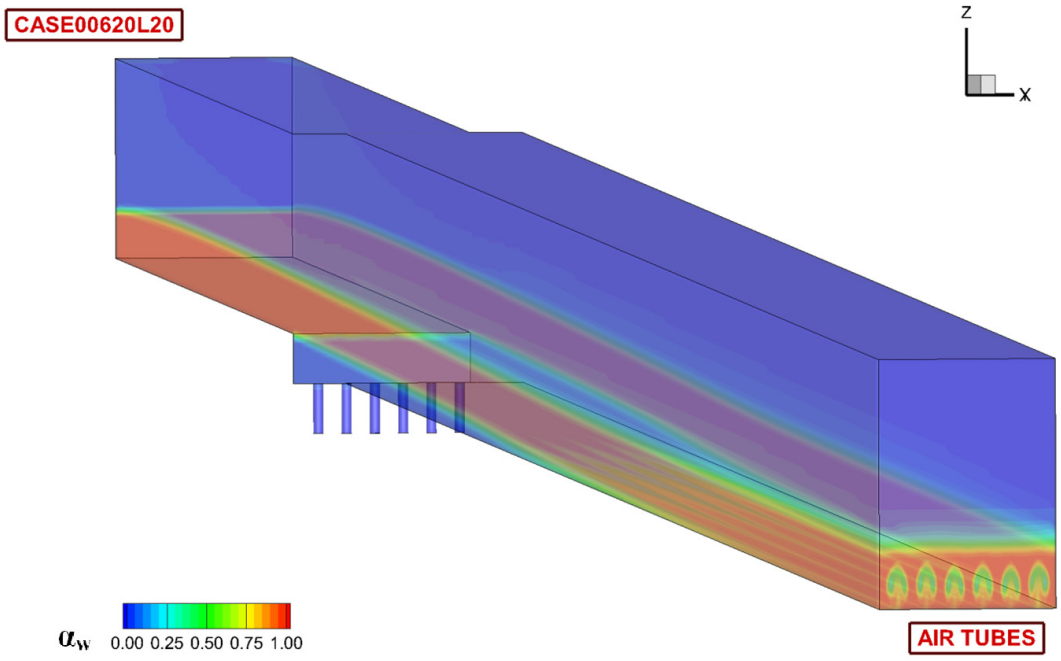

Figure 4.1: Visualization of the flow using α_w values. Blue areas are completely filled with air, while the red areas represent the presence of water. The air-water mix is shown by the colour scale given.

The aeration of the flow takes place over the step as shown in Figure 4.1. The regions in the domain that are majorly occupied by the water are represented by red. The blue regions represent presence of air phase. The other regions where cyan, green and yellow contours of α_w values are observed are the regions where air and water phases are mixed. The presence of step creates an aeration chamber under the jet. The circular shaped air ducts introduces air to the flowing water as the flow jets off the step. The air entrained in the flow causes formation of circular shaped air tubes that remain visible over the span of the domain until the outflow boundary. The jetting water reattaches to the channel bottom after certain distance. This distance measured from the beginning of the step till the reattachment point is referred as jet-length in the present study. After the reattachment point over the bottom boundary the air tubes form stripes of low density regions with low velocities which act as a protection layer against cavitation.

In the simulations the total incoming air flow is recorded at the lower boundary of the air ducts. The simulations are assumed to reach a steady state when the airflow reading at each simulation reaches to a constant value. These values represent the amount of air introduced to the water flow at the downstream of the ducts and they are given in Figure 4.2. The initial oscillation in air flow, which is observed in all the simulations, is due to the fact that all the simulations start with a domain full of air and part of the air escapes through these ducts and the outflow boundary as the water enters the domain through inlet. After these initial oscillations the airflow reaches a steady state at about t =7.0 s for almost all the simulations. Based on the final Q_{air} values at the end of 1000 time steps, β index of each flow is calculated.

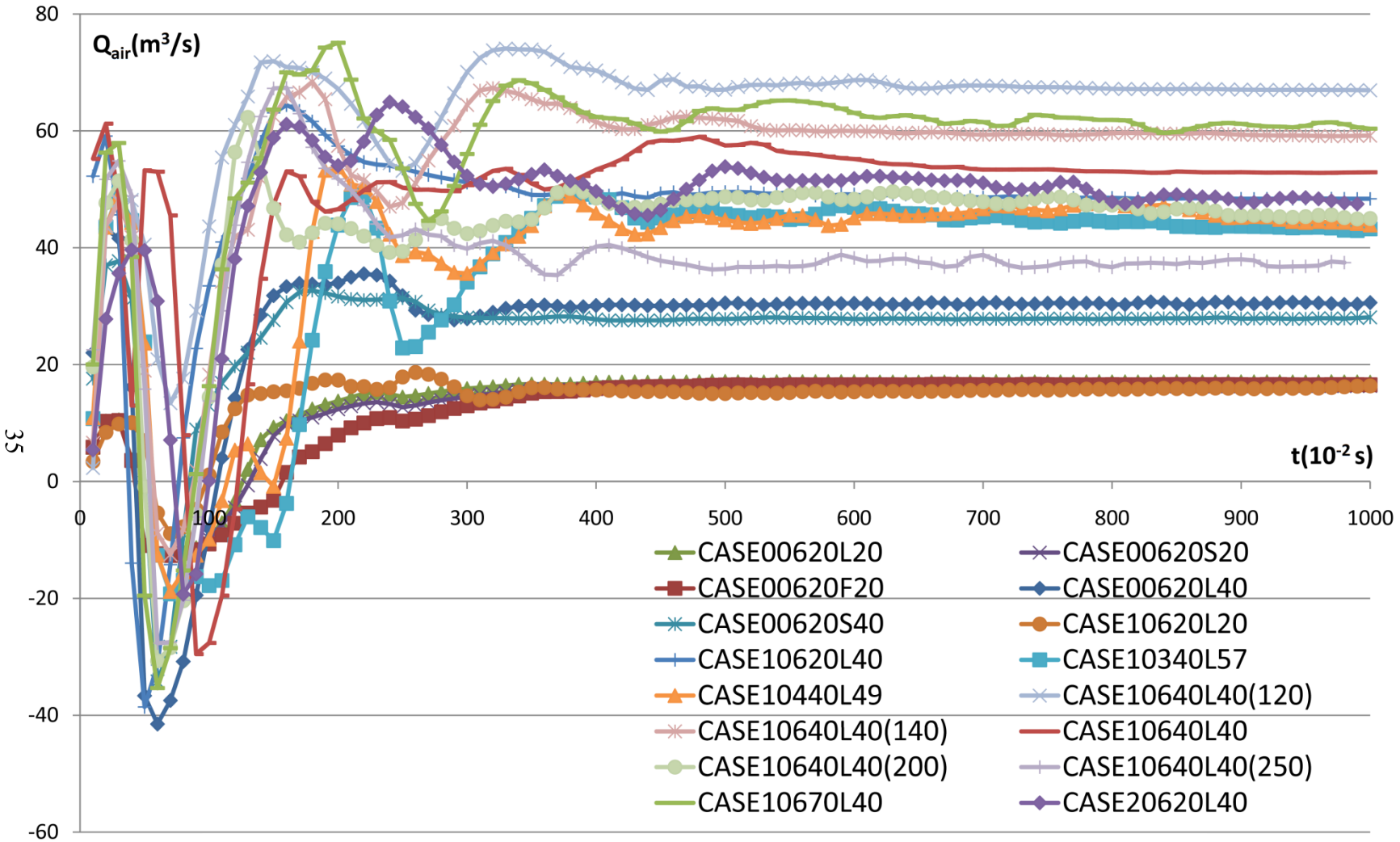

Figure 4.2: Temporal variation of total air inflow through the ducts for all simulations

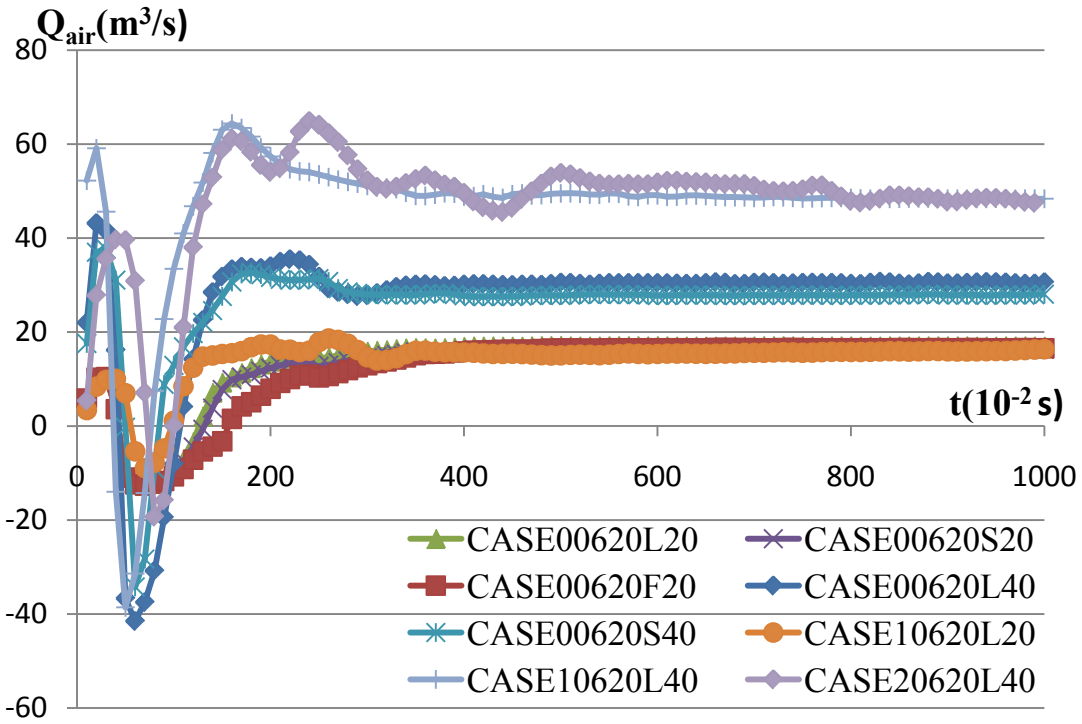

Figure 4.3: Temporal variation of total air inflow through the ducts for simulations with inflow discharge of 20 $m^3/s/m$

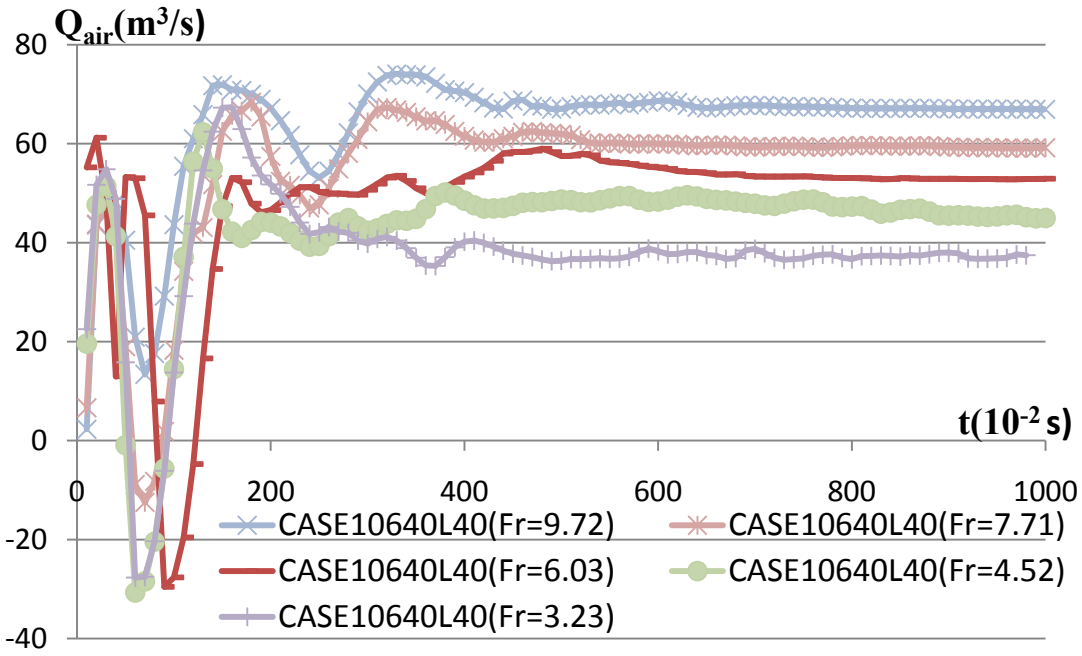

Figure 4.4: Temporal variation of total air inflow through the ducts for simulations with inflow discharge of 40 $m^3/s/m$, ramp height of 10 cm and duct diameter of 40 cm with *Fr*=3.23, 4.52, 6.03, 7.71, 9.72

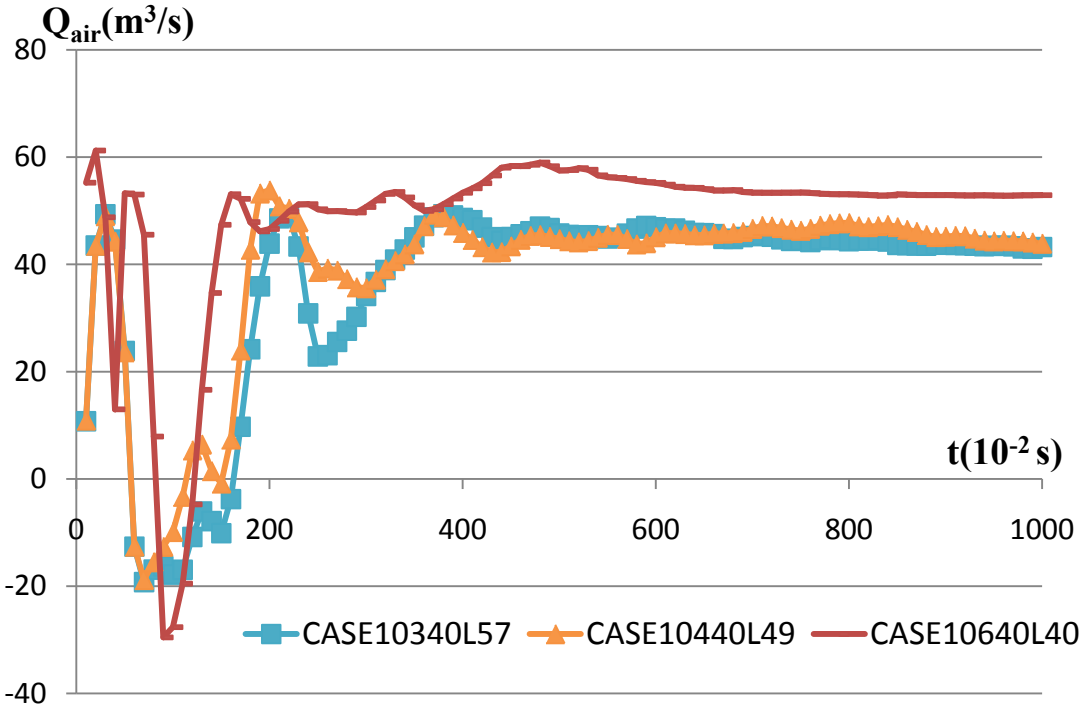

Figure 4.5: Temporal variation of total air inflow through the ducts for simulations with inflow discharge of 40 $m^3/s/m$, ramp height of 10 cm and varying duct diameters of 40 (total of 6 ducts), 49 (total of 4 ducts) and 57 cm (total of 3 ducts)

The same plot can be reduced and drawn for selected cases for preliminary observations. Cases with common unit discharge at the inlet of 20 $m^3/s/m$ are given in Figure 4.3. Based on this figure, steady-state aeration is nearly same for Cases 00620L20, 00620S20, 00620F20 and 10620L20. The duct diameters are same for these cases; location of ducts and ramp height are the variables. For larger ducts (Cases 00620L40, 00620S40, 10620L40, 20620L40), effect of presence of ramp can be seen independent of its height. In Figure 4.4 effect of Froude number can be seen for the Cases of 10640L40; where unit discharge at the inlet is 40 $m^3/s/m$ but flow depths and velocities vary. In the Figure 4.5 Cases 10640L40, 10440L49 and 10340L57 are presented; where air ducts have same total area in all the three cases however, the number of ducts are different in each case. In the figure it can be observed that total air entrainment to the domain is maximum with maximum number of ducts.

In the next sections the effects of all the geometrical variables on jet-length and flow aeration are discussed in detail.

4.2 Effect of Aerator Location, Aerator Size, Ramp Height and Discharge on Jet-Length and Flow Aeration

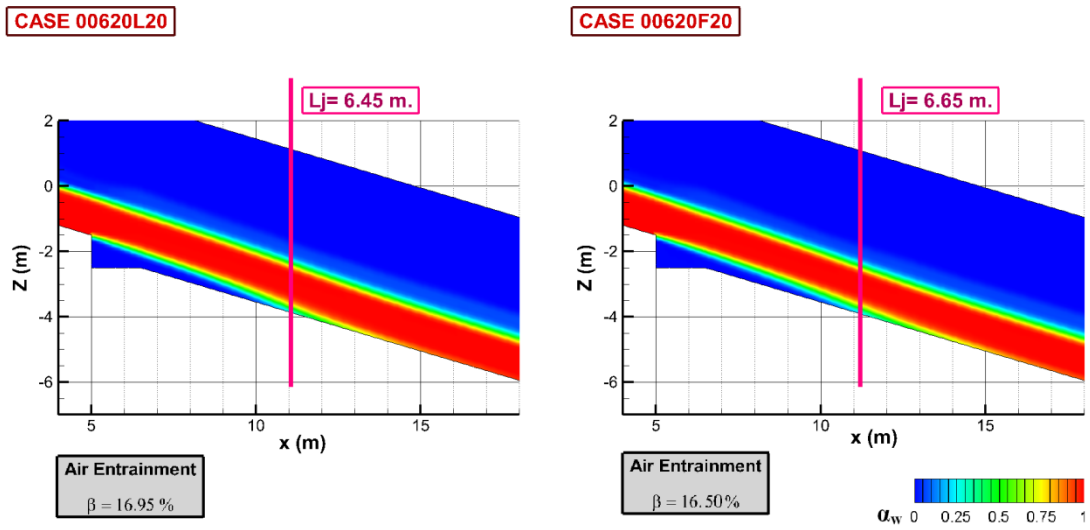

Figure 4.6: The water phase and jet-length visualization for Case00620L20 and Case00620F20

The centreline symmetry y-plane from each simulation is used for visualization of the flow and comparison of the results. The comparison between the Cases 00620L20 and 00620F20 in terms of jet-length and water surface profile is shown in Figure 4.6. These simulations have common unit discharge at the inlet of 20 $m^3/s/m$. They both lack of a ramp at the approach of the step and in both simulations the aeration was possible via six 20 cm-diameter circular air ducts placed over the step. However, the position of these ducts are different as in L20 case, all six of these ducts are placed in a line after a short distance from the vertical wall of the step while in the F20 case, the ducts are placed in a staggered fashion and three of them are placed in a line off the same distance from the vertical wall of the step and the other three are placed at the far end of the step where step ends and the channel begins (please refer to Figure 3.6 for the top view of the duct positioning). This change in

the positioning of the ducts forces the flow to have a relatively longer jet-length. The jet-length is measured such that the reattachment point is assumed to be at α_w=0.25 near the bottom of the channel after the aeration zone. The jet-length is about 6.45m in L20 simulation while the jet–length is found to be 6.65m in F20 simulation. However, no significant difference in terms of aeration is observed. Both cases have β index of about 16-17%. Even though the jet-length is somewhat increased with the far and staggered positioning of the aeration ducts over the step, one can state that the aeration is slightly reduced. The water surface profile in both cases remains unchanged. Top of the water jet runs parallel to the channel bottom. The extent of the aerated bottom chamber is slightly longer in F20 case, reaching until x>15 m, while for L20 case it is x<15 m.

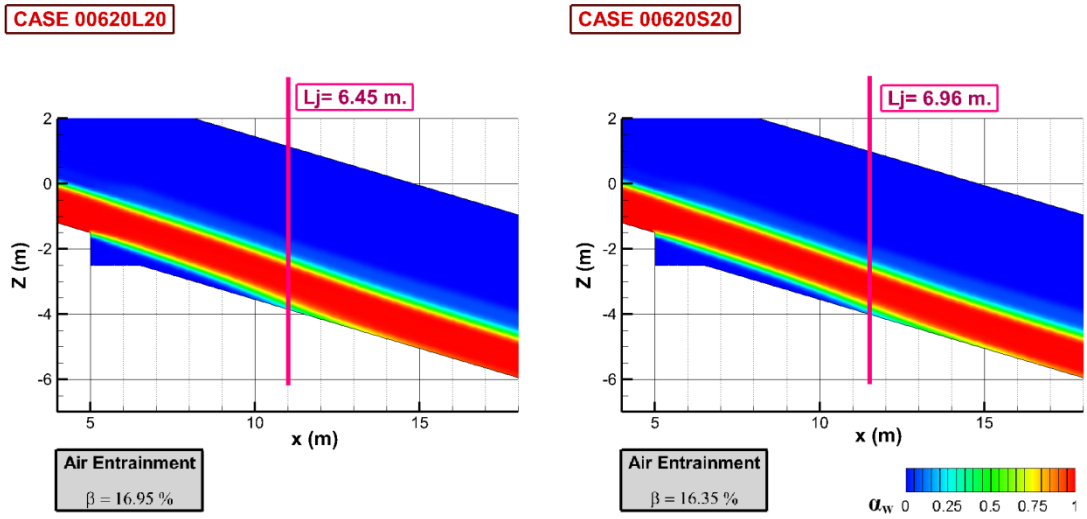

Figure 4.7: The water phase and jet-length visualization for Case00620L20 and Case00620S20

Interestingly, if the staggered ducts are not placed so far apart from each other their effect on jet-length becomes much more pronounced almost with no change in air entrainment index compared to L20 case. Figure 4.7 shows the Case00620L20 together with Case00620S20. In the case of S20, the aeration ducts are also placed in

a staggered fashion over the two lines. Each line has 3 air ducts. The distance between these lines is almost equal to the length of the step in F20, while the distance between the lines of three is very small and is only about 10 cm in S20. When the distance is very small between these lines such that it is comparable or smaller than the duct diameter itself, the ducts act as if their surface area has increased. Their combined effect pushes the water further over the step. The jet length L_j = 6.96 m in the case of S20, which is higher than both L20 and F20. Moreover, aeration index β for L20 and S20 is about 16-17%.

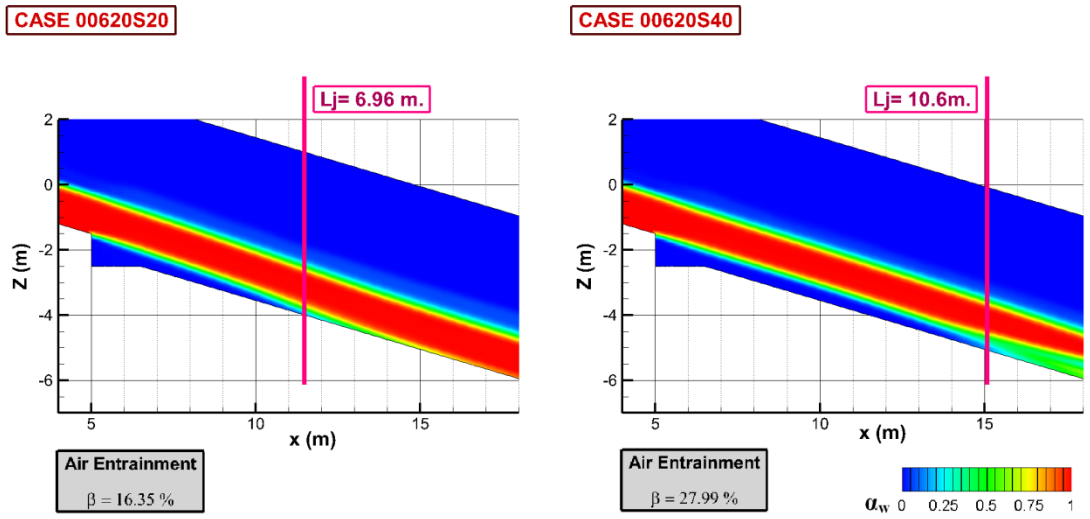

Figure 4.8: The water phase and jet-length visualization for Case00620S20 and Case00620S40

In the Figure 4.8 two staggered simulation cases are compared. Both simulations have the same inflow parameters, no approach ramp and same number of air-ducts. However, the air duct size is twice in Case00620S40. In both staggered simulation cases the ducts are placed in two rows. Each row similar to previous "S" cases has three ducts. In both simulations the rows are of the same distance apart. However, when the diameter of the air ducts increases, the air entering to the domain through each duct interpenetrates to the neighbouring one and forms larger air tubes compared to single air tubes that form in "L" simulations. The jet-length and air

entrainment increases mainly due to presence of larger air ducts in S40 case. However, another significant observation is the formation of the highly aerated mixed flow regions on wider stretches over the spanwise direction near the bed as shown in Figure 4.17. This will be discussed further in Section 4.5. The highly aerated flow region is mostly visible if one compares the downstream composition of the flow by looking into the near bottom α_w values after the reattachment point in Figure 4.8.

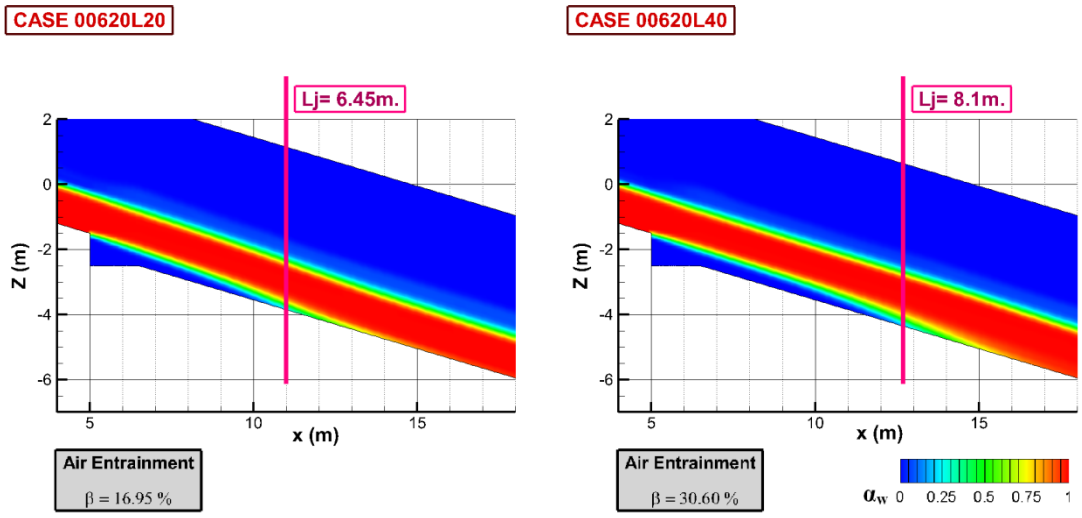

Figure 4.9: The water phase and jet-length visualization for Case00620L20 and Case00620L40.

In the Figure 4.9, the effect of size of aeration ducts is shown. In both simulations the incoming water discharge is 20 $m^3/s/m$ and both simulations are lack of a ramp at the approach of the step. Both simulations use six aeration ducts over the step and they are positioned same distance from the back wall of the step. However L40 case has 40cm-diameter ducts while the L20 uses 20cm-diameter ducts. Larger size of the aeration ducts allows flow to have longer jet-length as well as higher aeration index β. The aeration in L40 case is almost doubled and jet length increases about 1.25 times compared to L20 case. The water surface profiles reveal that due to higher aeration in L40 case, on the downstream side after the reattachment to the channel

bottom, the depth of the air mixed flow increases about 27 cm compared to L20 case. The depth of the flow in L20 is about 1.34 m, while the depth of the flow in L40 is about 1.61 m at x= 15m. As expected the size of the aeration zone under the jet is longer for L40 case.

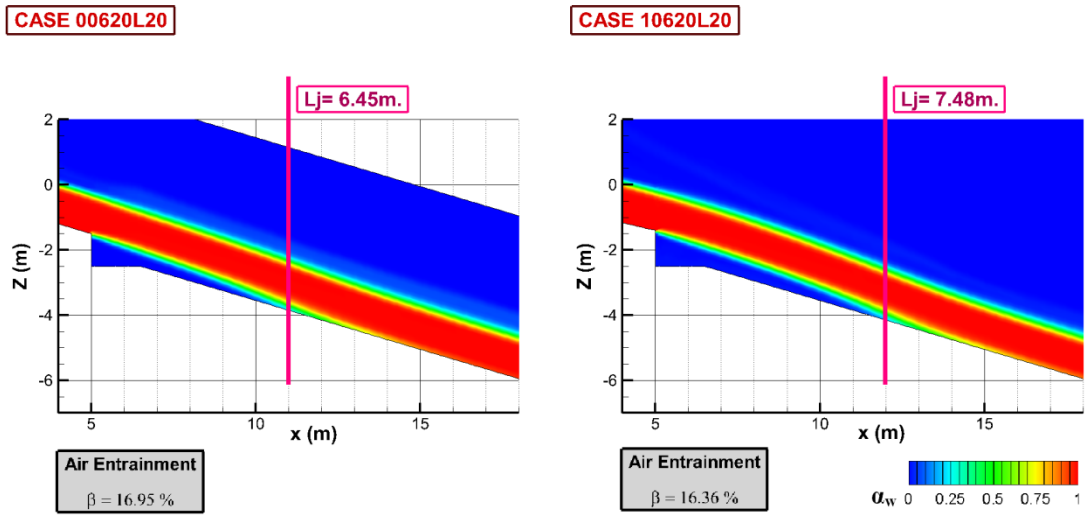

Figure 4.10: The water phase and jet-length visualization for Case00620L20 and Case10620L20

The effect of the ramp is also evaluated in the simulations by using two different ramp heights at the approach of the step. Figure 4.10 shows the effect of ramp in comparison to no ramp case. Both simulations have same inflow discharge and same number and size of air ducts. However Case10620L20 has a 10 cm high ramp at the approach of the step as opposed to lack of a ramp in Case00620L20. The ramp shows its effect in the upper water-air interface as seen in the figure. The jet lifts off higher in the presence of a ramp and this also affects the length of the jet which increases almost about a meter by the help of 10 cm high ramp. This ramp height is observed to have no effect on the aeration index β of the flow in the case of inflow discharge of 20 $m^3/s/m$.

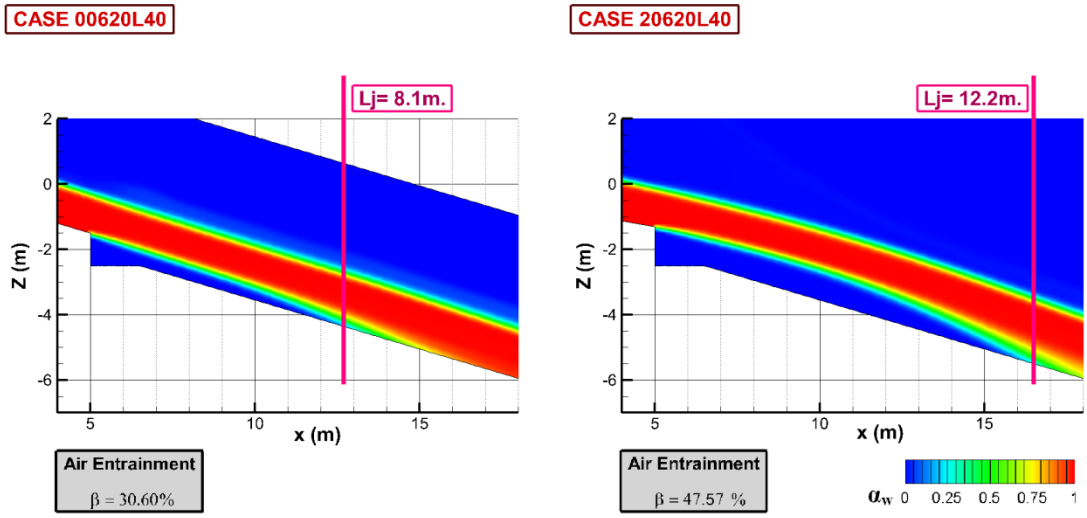

Figure 4.11: The water phase and jet-length visualization for Case00620L40 and Case20620L40

The higher the ramp height, the greater the change observed of jet-length and the air entrainment. The air entrainment increases from 30.6% to 47.6% when the ramp height increases from 0 to 20 cm for the simulations with 20 m^3/s/m inflow and six 40 cm diameter air ducts. The length of the jet increases about 4m with the 20cm high ramp, which can be seen in Figure 4.11. The trajectory of the jet also changes quite dramatically allowing much larger volume of aeration zone over the step under the jet. Depth of the flow downstream of the reattachment at x=20 m is about 1.49 m for case with no ramp while with the ramp the depth increases to 1.83 m. This is basically due to the entrained air, which increases the total volume of the flow.

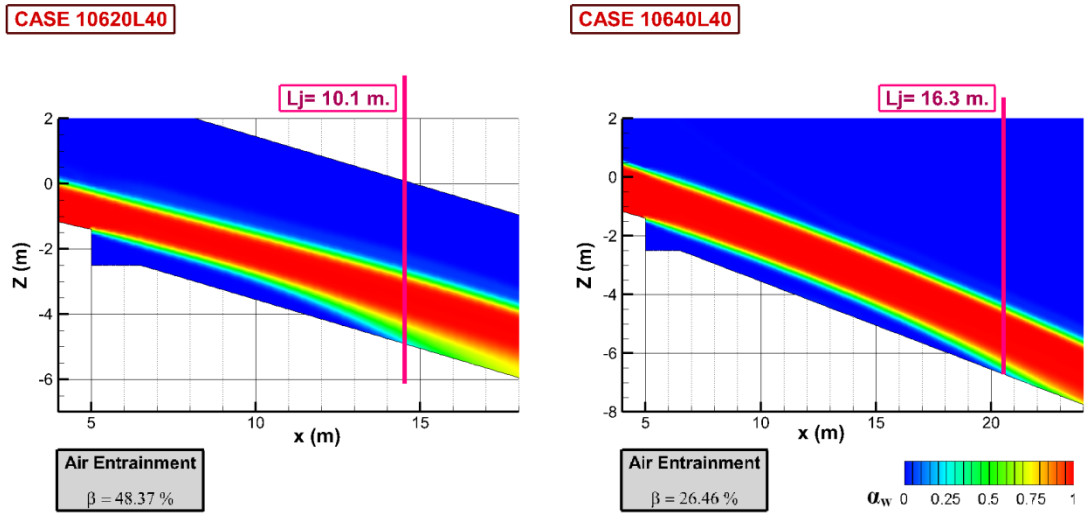

Figure 4.12: The water phase and jet-length visualization for Case10620L40 and Case10640L40

The effect of higher discharge is visible in Figure 4.12. The discharge is twice larger in Case10640L40. The larger discharge causes jet-length to increase, the jet length increases about 6 m as the discharge is doubled. Doubling the discharge while keeping the size and number of air ducts constant causes a drop in air entrainment form 48.37% to 26.46% as observed in the previous experimental studies. This is majorly due to the definition of the air entrainment which involves the ratio between incoming water flow and recorded air flow into the domain through the ducts.

One can also compare Figure 4.12 with Figure 4.11 to observe the effect of 10 cm high ramp on the flow when the discharge is only 20 m^3/s/m. The 20 cm high ramp pushes the flow 4 m further downstream in terms of jet-length while 10 cm high ramp pushes the flow 2 m further downstream compared to the case with no ramp. Therefore, the increase in ramp height almost has a direct effect on the jet-length if all the other parameters are kept constant in the simulation setup.

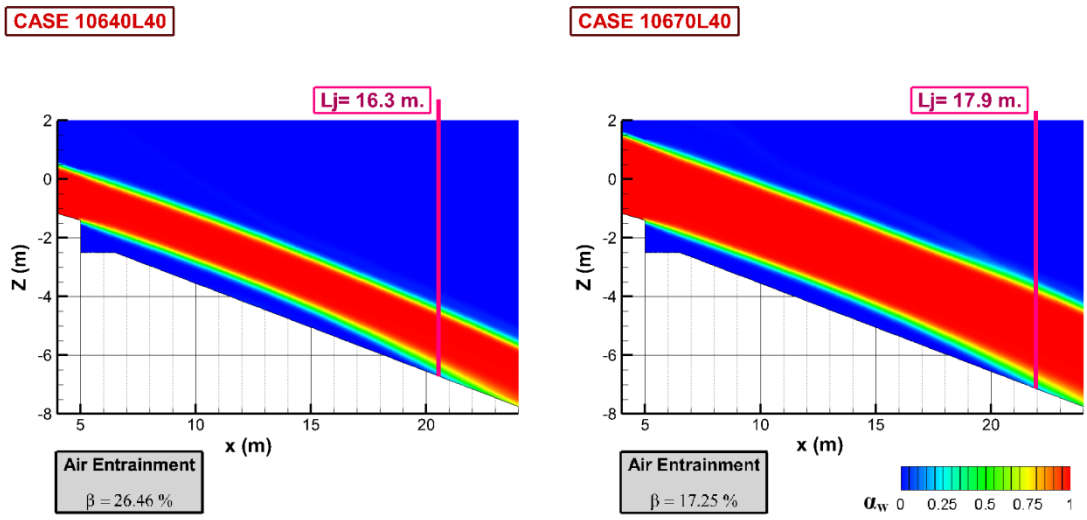

Figure 4.13: The water phase and jet-length visualization for Case10640L40 and Case10670L40

With further increase in discharge one can expect to see proportional increase in the jet-length. However, the jet-length depends more on the velocity of the flow rather than the discharge itself. In case of 10670L40 the inflow discharge has increased 1.75 times the case of 10640L40. Figure 4.13 shows the comparison. However, the increase of the discharge is due to increase in both flow velocity and also in flow depth at the inlet section as the discharge is defined as the multiplication of the water flow area and average velocity through that area. Therefore, in the case of 70 $m^3/s/m$ inflow discharge, one can observe an increase in the jet-length to 17.9 m compared to the jet length of 16.3 m in 40 $m^3/s/m$ inflow case, however this increase is not proportional to the increase that is observed between the cases 10620L40 and 10640L40. Therefore, it is also important to consider the combined effect of velocity and depth of the flow through Froude number. In the next section, Froude number effect on the jet-length as well as on the aeration is discussed.

4.3 Effect of Inflow Froude Number over the Flow Aeration and Jet-Length

Same inflow discharge with various Froude numbers is possible if one changes the average velocity and flow depth at the inflow boundary. The Froude number is defined as the ratio between the inertia force and the gravitational force as given in Equation 4.1. In the present study, Fr number is calculated for flow over the ramp or step.

$$Fr = \frac{V_{ramp}}{\sqrt{g h_{ramp}}} \tag{4.1}$$

In this equation V_{ramp} represents the average cross-sectional velocity of the flow over the ramp or step, g represents the gravitational acceleration and h_{ramp} represents the depth of the flow over the ramp or step. The significance of the Froude number is that it shows what type of hydraulic communication exists between the upstream and the downstream of the flow. If the Froude number is greater than 1, the flow is called supercritical flow. In these types of flow any kind of disturbance to the flow at the upstream could be carried to the downstream.

In the current study, all the simulations conducted are in the supercritical range; however the ones that are discussed so far have Froude numbers between 5.04 and 6.03. In this section, five simulations that are presented have a constant inflow discharge of 40 $m^3/s/m$; contrary to the previous results these simulations have the range of 3.23-9.72 for the Froude number. The highest flow velocity and hence the lowest flow depth at the inflow section is observed for *Fr*=9.72 In this case the average flow velocity is taken as 33.33 m/s and the depth of the flow is 1.2 m at the inlet. When *Fr*=3.23, the average flow velocity and the depth at the inlet is 16 m/s and 2.5 m, respectively.

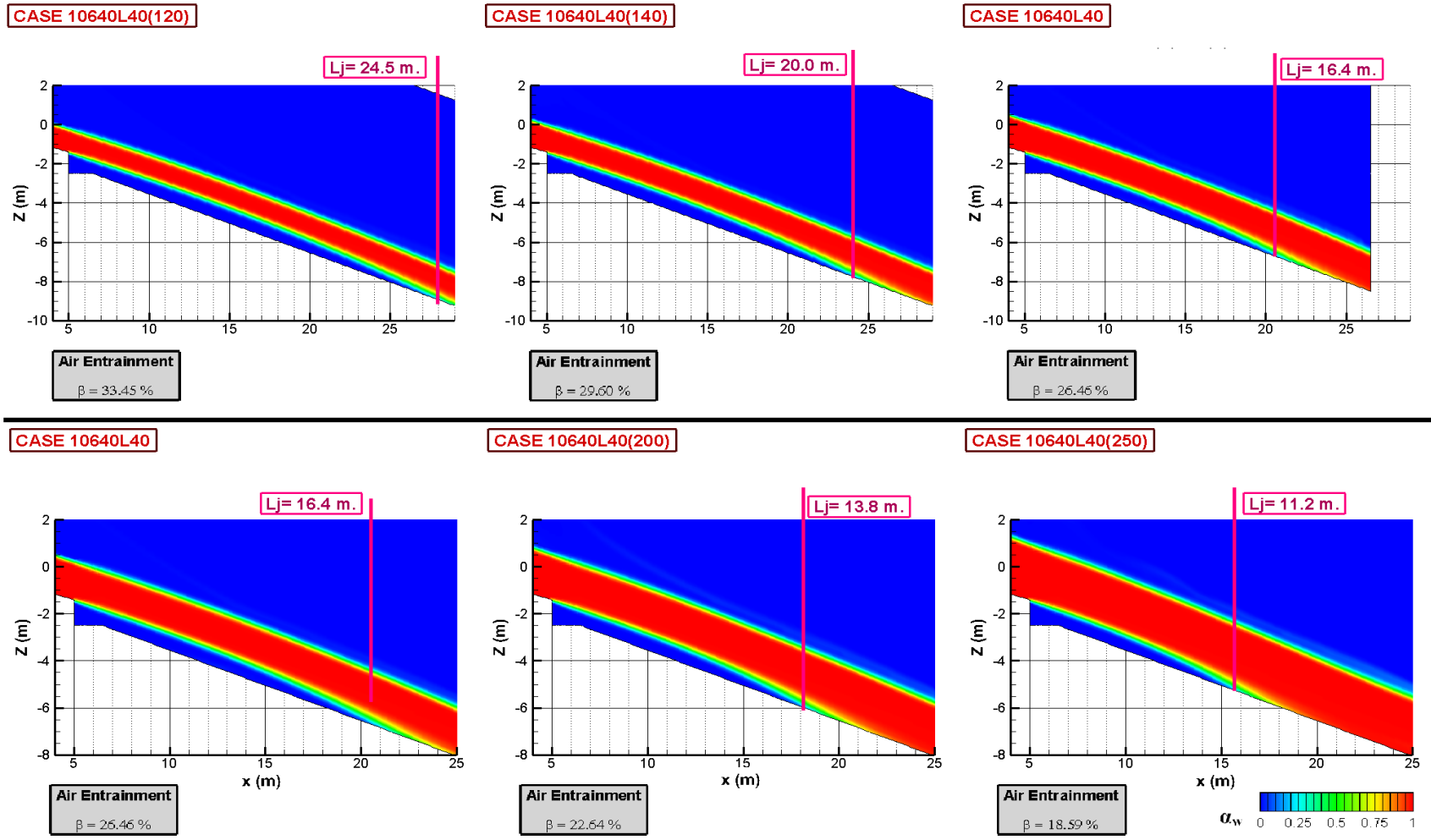

Figure 4.14: The water phase and jet-length visualization for Case10640L40(h_{inlet}=1.2m, *Fr*=9.72), Case10640L40(h_{inlet}=1.4m, *Fr*=7.71), Case10640L40(h_{inlet}=1.65m, *Fr*=6.03) Case10640L40(h_{inlet}=2.0m, *Fr*=4.52), and Case10640L40(h_{inlet}=2.5m, *Fr*=3.23)

The jet length is observed to increase quite significantly as the Froude number increases as given in Figure 4.14. Even though in all the simulations a ramp with height of 10 cm is used, the ramp is not observed to change the trajectory of the flow significantly in high Froude number simulations. In the high Froude number cases the inertia force dominates the flow. Therefore, the effect of gravitational force is far less significant in high Froude cases; this causes almost straight looking water-air interfaces at the top of the jet. As the Froude number gets smaller the jet is observed to have curved upper and lower water-air interface due to the presence of a ramp at the approach of the step.

The smallest jet-length observed is about 11.2 m for the lowest Froude number case. The largest jet-length is about twice larger at around 24.5 m compared to lowest Froude number case. This jet length is observed when the depth of the inflow is almost half of the one in lowest Froude number simulation.

The relation between Froude number and jet-length is shown in Figure 4.15. The jet-length increases with increasing Froude number. The trendline shows that relative jet-length is a function of $Fr^{1.75}$ similar to the empirical equation suggested by Kökpınar and Göğüş (2002) based on their experimental study. In Table 4.1 the values of aeration with respect to Froude number is listed for these simulations. As the Froude number increases the value of the aeration index β also increases. The aeration reaches 33.45% at highest Froude number simulation, while it drops down to 18.59% at the lowest Froude number simulation.

Table 4.1: β and L_j / h_{ramp} change with respect to Fr

Case	Fr	L_j / h_{ramp}	β (%)
10640L40(120)	3.23	4.48	18.59
10640L40(140)	4.52	6.90	22.64
10640L40	6.03	9.91	26.46
10640L40(200)	7.71	14.29	29.60
10640L40(250)	9.72	20.17	33.45

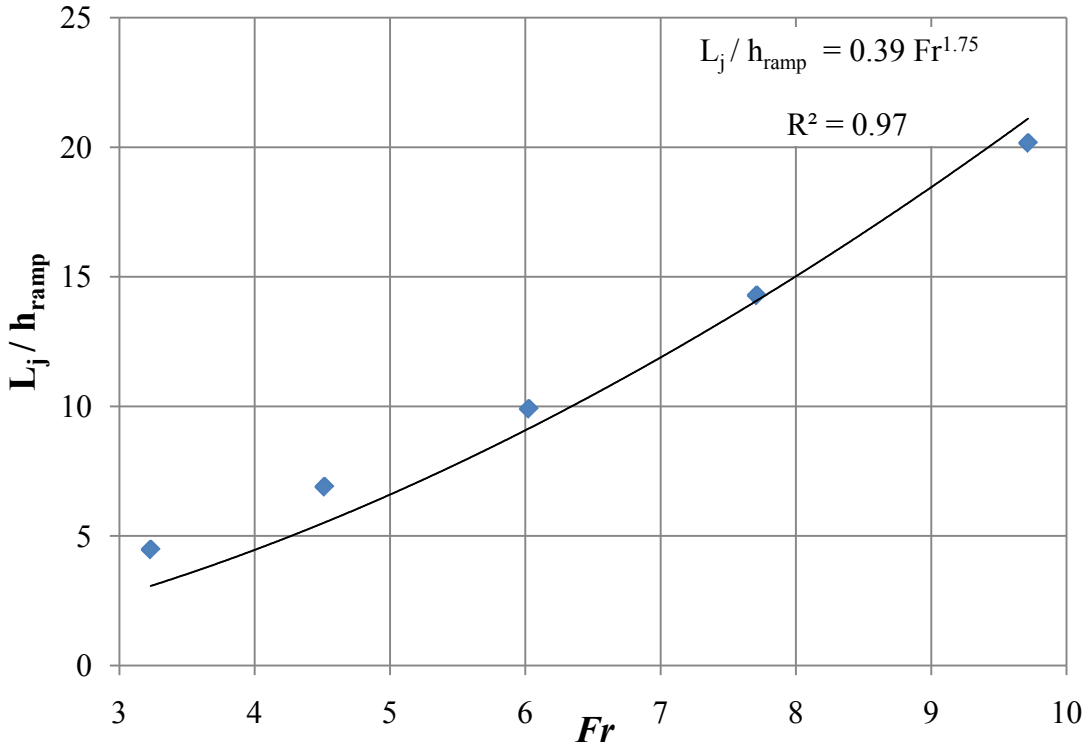

Figure 4.15: Change in jet-length with respect to Froude number of the flow upstream of the step

4.4 Effect of Number of Aerators on the Jet-length and Aeration

In order to assess the effect of number of aerators on the jet-length and aeration, two variations to Case 10640L40 are investigated. The total area of the air ducts is calculated based on Case 10640L40, where six ducts with each of them having diameter of 40 cm are used. Then, the diameters of the aerators are increased to 49cm (Case 10440L49) and 57 cm (Case 10340L57) in two separate simulations, while keeping the total aeration area constant. As the diameter of single aerator increases, the number of the aerators that is needed to satisfy the above condition decreases. Therefore, in the simulation where single aerator diameter is 49 cm, total number of aerators is 4, and in the simulation where single aerator diameter is 57 cm, total number of aerators is 3. These air ducts are placed over a line at the same location

over the step as in case of L40. The other geometrical parameters of the simulations are unchanged. The inflow discharge in all the three simulations is 40 $m^3/s/m$. In the case of L49, the jet-length increases quite significantly from 16.3 m to 20.5 m compared to L40 case. However, in the case of L57, the jet-length is measured as 21.6 m, closer to the value observed in L49 simulation. It is also important to note that the aeration index β decreases with a decrease in number of aerators. The β index in L40 simulation is found to be 26.45%, while β index is around 22% in both L49 and L57 simulations. The comparison is given in Figure 4.16.

This decrease in the aeration index compared to "L" cases is also observed in the scattered configuration of the air ducts, where the distance between two rows of ducts is so small that the air stream from each duct interpenetrates. Especially in the case of 40 cm diameter air ducts, two neighbouring duct behaves as one big duct, where the β index drops down to 27.99% compared to 30.60%. In the next section, further effects of interpenetrating air streams are discussed.

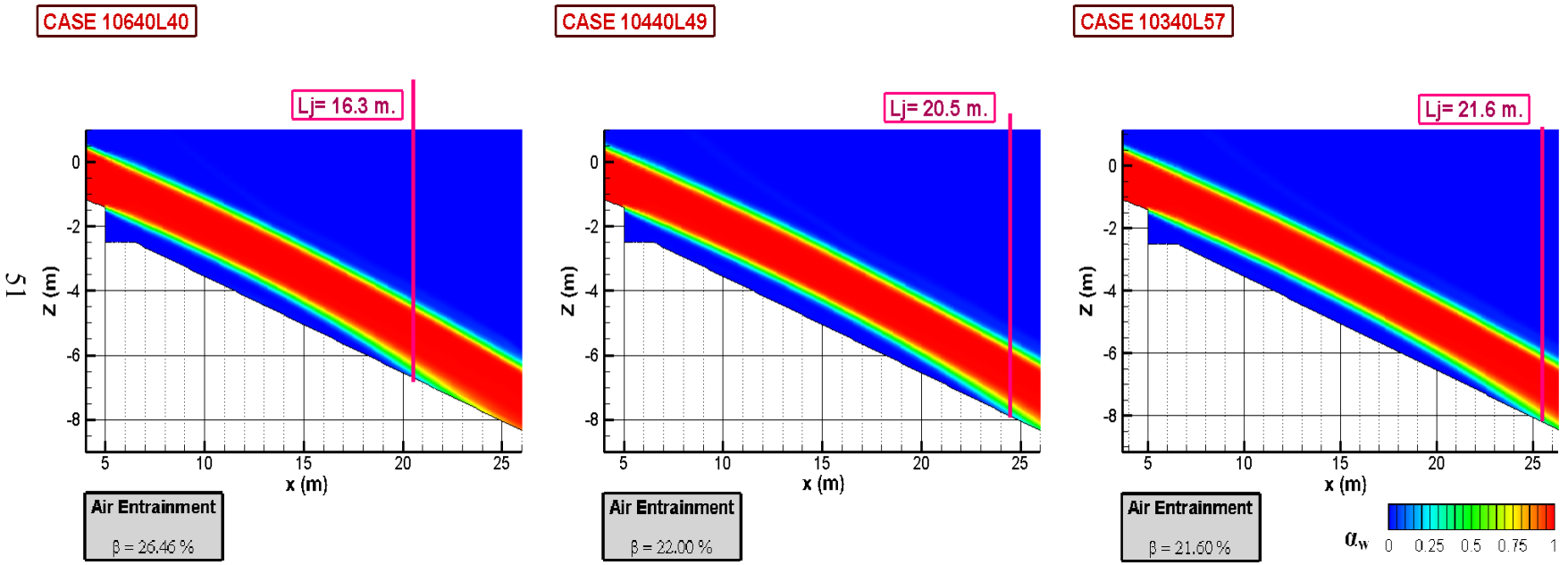

Figure 4.16: The water phase and jet-length visualization for Case 10640L40, Case 10440L49 and Case 10340L57

4.5 Interpenetrating Air Tubes and Their Effect Near the Channel Bottom

As mentioned earlier, the interpenetrating air tubes appear in the scatter configuration of the air ducts on the step. The distance between the rows of air ducts is only about 10 cm in the "S" simulations of 20 cm diameter cases and 40 cm for 40 cm diameter cases. This causes air streams from neighbouring air ducts to interact, especially when the diameter of the air ducts are 40 cm However, similar phenomena is also observed for cases with air duct diameter of 20 cm.

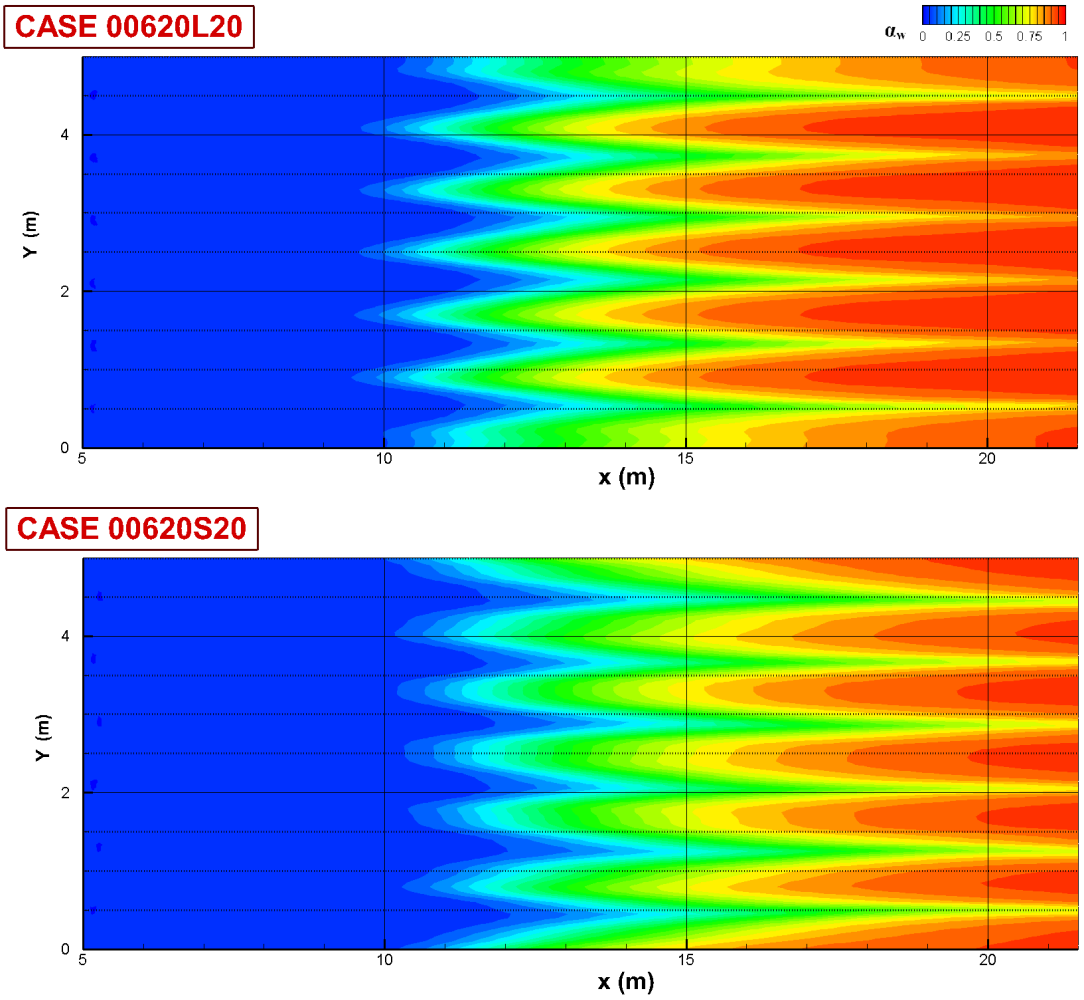

Figure 4.17: The mixed air-water phase distribution over the span of the spillway near the channel bottom for Case 00620L20 and Case 00620S20

Figures 4.17 and 4.18 show a plane parallel to the channel bottom. The plane is 5 cm away from the bottom. Over this plane the air-water phases are visualized using α_w values. In Figure 4.17 results from small size air duct simulations are presented. In both L20 and S20 cases, over the span one can observe formation of high and low α_w stripes. The low α_w stripes show the trajectory of the air tubes. In case of S20, both the width and length of these stripes are observed to be longer than the ones observed in L20 case. In L20, α_w value of 0.5 permeate until about x=17-18 m, while in S20, it surpasses x=20 m. Similar observation is possible for α_w value of 0.25. In L20, α_w=0.25 extends only until x=15 m, however in S20, α_w =0.25 creeps until x=17 m.

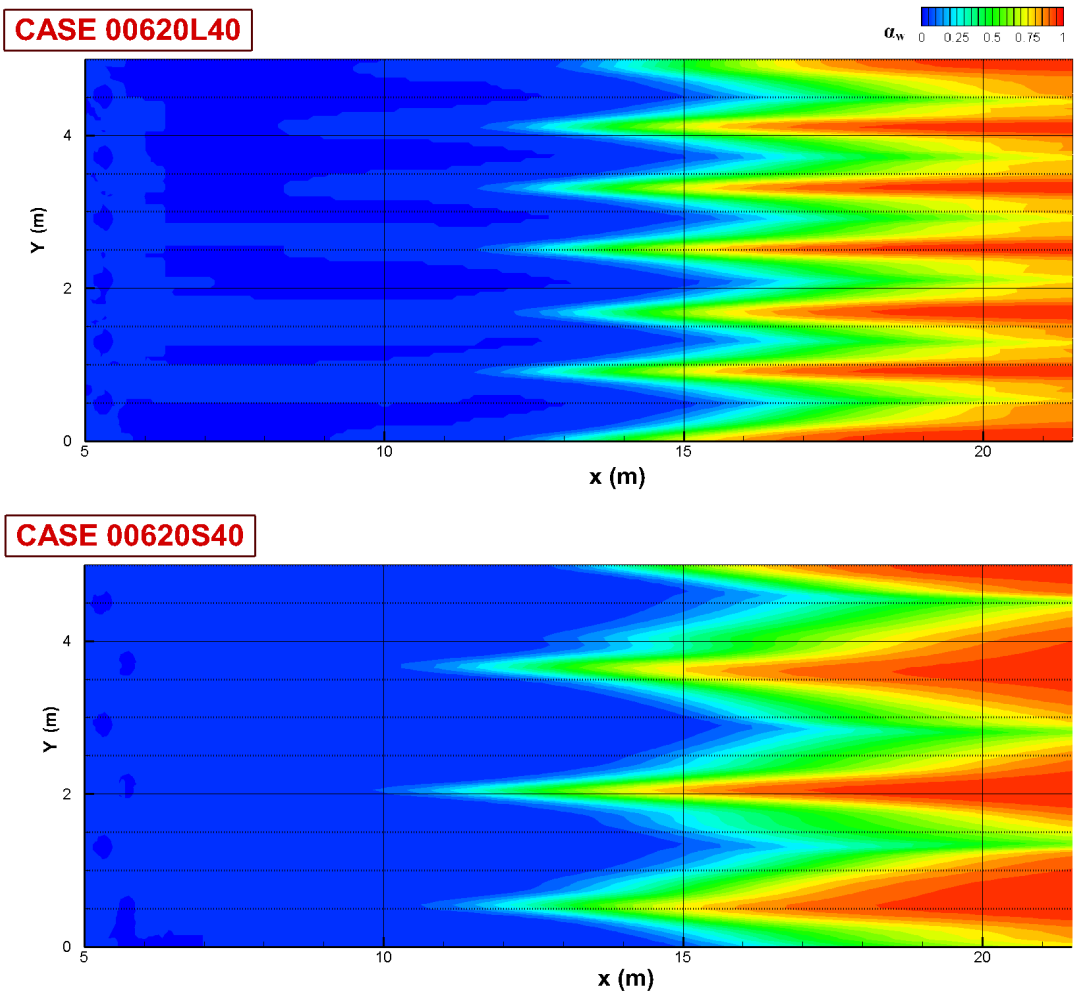

Figure 4.18: The mixed air-water phase distribution over the span of the spillway near the channel bottom for Case 00620L40 and Case 00620S40

The effect of these combined streams of air is far more visible in the case of larger diameter air ducts. In the L40 case given in Figure 4.18, one can still observe the formation of well-defined six separate air tubes from the striped trajectories that they form near the channel floor. In the case of S40 however, only three separate air tube tracks are visible between four water dominated regions near the channel floor. This shows how two neighbouring air ducts work as one big air duct and in a sense decrease the total number of air ducts used in the simulation S40. Hence, the decrease in aeration for S40 case compared to L40, similar to the decrease observed in the previous subsection.

4.6 Variation of Velocity Magnitude over the X-Planes Downstream of the Reattachment Point

Figure 4.19 shows the variation of cross sectional velocity magnitude at four different x-planes in three different simulations (Cases 10640L40, 10440L49, 10340L57). These planes are taken at the end of the simulation time when flow has already reached a steady-state. First plane given in Figure 4.18a is taken close to the reattachment point of the jet. Then three more planes are taken 1.5 m (frame b) , 3 m (frame c) and 4.5 m (frame d) away from this first plane in the streamwise direction. The results show that over the channel bottom a protected layer of low velocity air-water mixed flow occurs. The protected layer has a thickness of about 50 cm. The values of velocity near the reattachment point inside this protected layer are about 5m/s or less. However, the shape of this protected layer is very much affected by the number and size of the aeration ducts used in the simulation. Despite the fact that total aeration area is common in all three simulations shown in the figure, when the distance between the aeration ducts increase due to simultaneous decrease in their number and increase in their size, the extent of the unprotected regions increases. In this regard, placing many aeration ducts side by side or having a continuous aeration opening over the full span of the spillway structure would create much uniform protected layer near the channel floor. The advantage of having many adequate size air ducts placed in closer distance to one after the other compared to single continuous opening for aeration might be the possibility of having higher β index due

to higher suction effect of jet when it passes over smaller size air ducts as discussed in Section 4.4.

The air mixed layer moves away from the channel floor as air raises to the free-surface due to its lower density compared to water. When air tubes move away from the channel bottom as one goes further downstream from the jet reattachment, the lower velocity layer also moves away from the bottom. The velocity values in the mixed protection layer also increases due to a decrease in the air concentration in this layer as one moves in the streamwise direction.

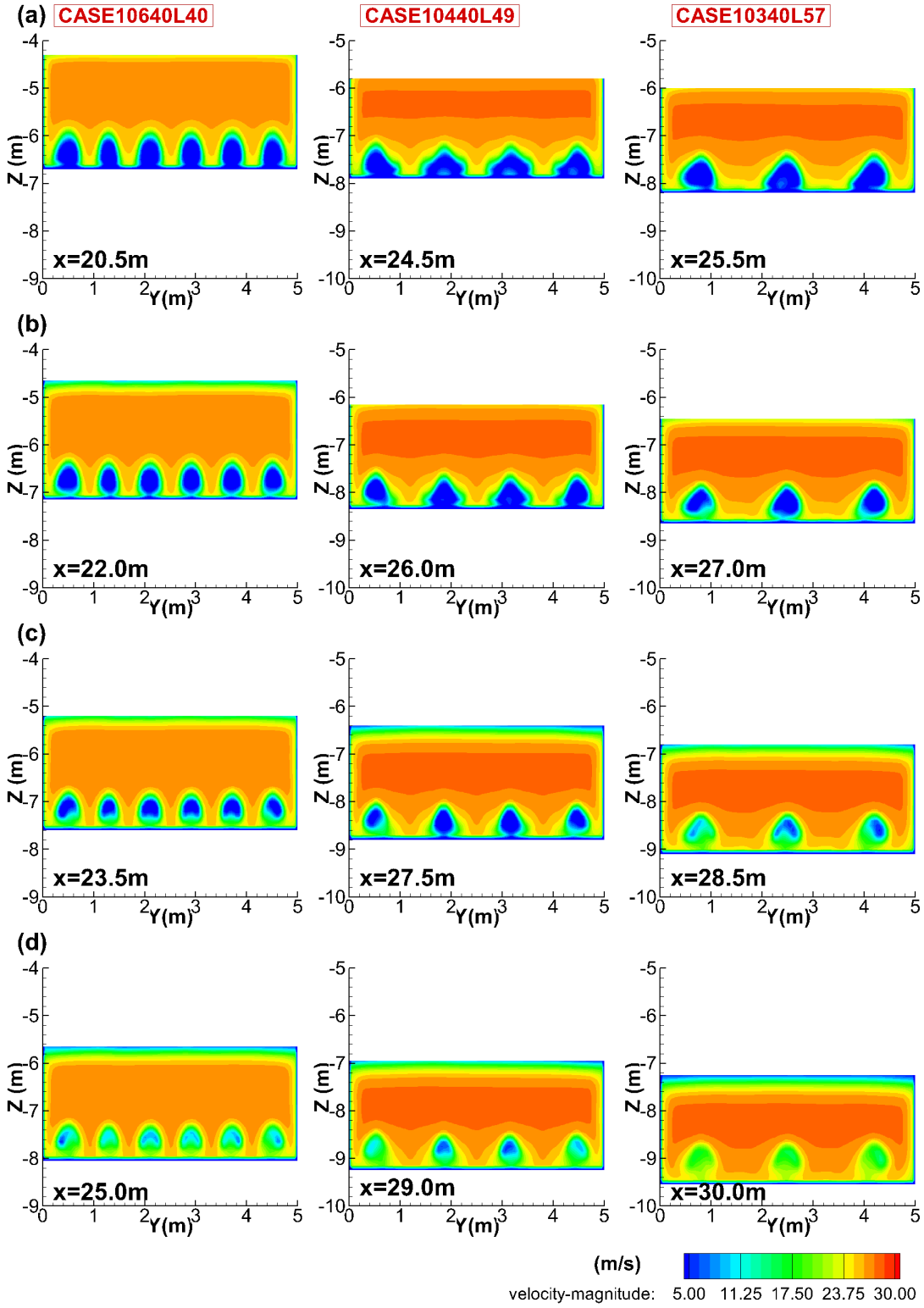

Figure 4.19: Variation of velocity magnitude over the x-planes downstream of the reattachment point for Case 10640L40, Case 10440L49 and Case 10340L57

4.7 Variation of Air Concentration in the Streamwise Direction

Cross sectional average of air concentration below the free surface of the flow is calculated over many x-planes in the streamwise direction after the reattachment of the jet. The interface between the air and water at the free surface is omitted in the calculations as the results concentrate on the air entrainment through the air ducts over the step in the lower nappe. The air concentration is observed to decrease as one goes away from the reattachment point towards the exit boundary. This is due to the fact that air escapes vertically as flow propagates further in the x direction. The decrease in concentration could be expressed with a logarithmic decay as shown in Figure 4.20 for all three cases with inflow discharge of 20 $m^3/s/m$. In these simulations, no ramp is used at the approach of the step and the diameter of the air ducts is 20 cm. In the concentration plots $x - x_i$ shows the distance from the reattachment point, x_i is the reattachment location of the jet to the channel floor. In these simulations, the relative location of air ducts is not observed to vary the average air concentration over the streamwise direction significantly.

Similarly, the average cross sectional air concentration values over several x-planes are calculated for the cases with inflow discharge of 40 $m^3/s/m$ with $3.23 \leq Fr \leq 9.72$. The diameter of the air ducts in these simulations is 40 cm. At the approach of the step there exists a ramp with height of 10 cm. The results are plotted both in normal and also in log-normal scale in Figures 4.21 and 4.22. In higher Froude number cases (Fr=6.03, 7.71 and 9.72) the decay is faster and changes with $(x - x_i)^{-1/20}$. In the cases of lower Froude number the decay is observed to be somewhat slower and varies with $(x - x_i)^{-1/33}$.

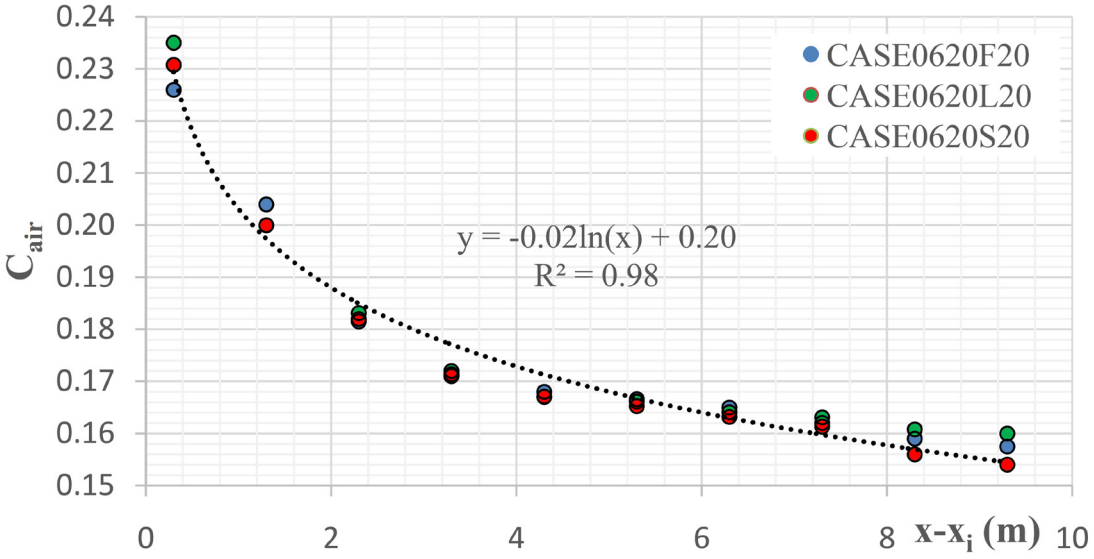

Figure 4.20: Cross sectional average air concentration at several streamwise locations for Cases 00620L20, S20 and F20

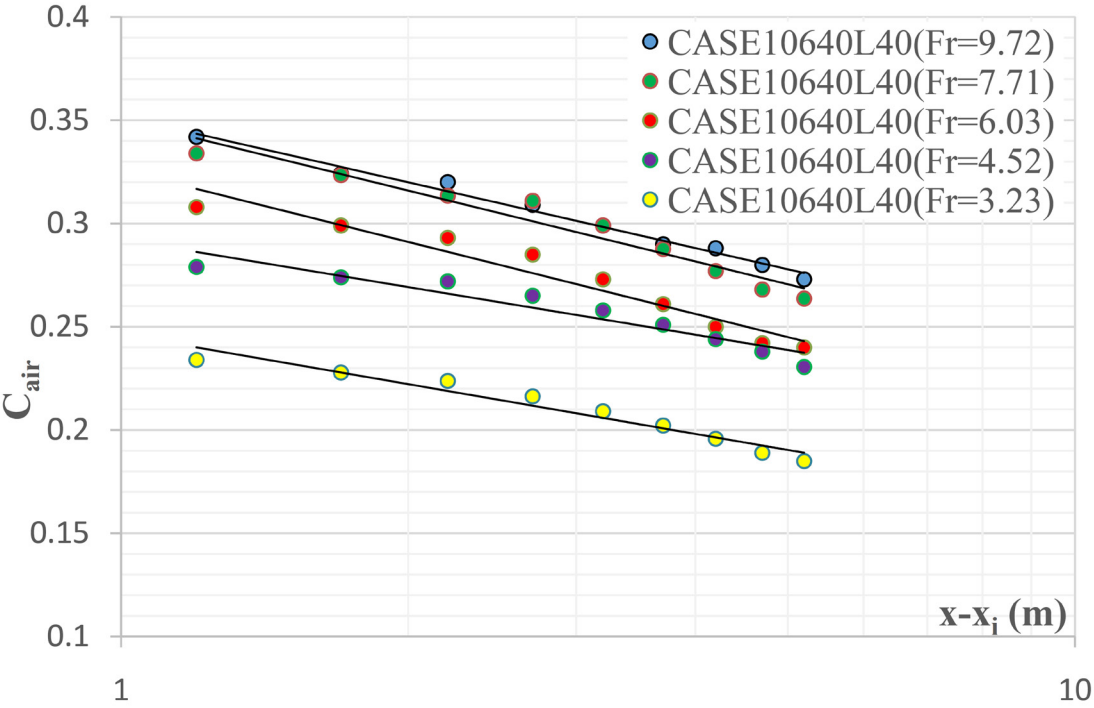

Figure 4.21: Cross sectional average air concentration at several streamwise locations for Cases 10640L40 with *Fr* = 3.32, 4.52, 6.03, 7.71 and 9.72 plotted in log-normal scale

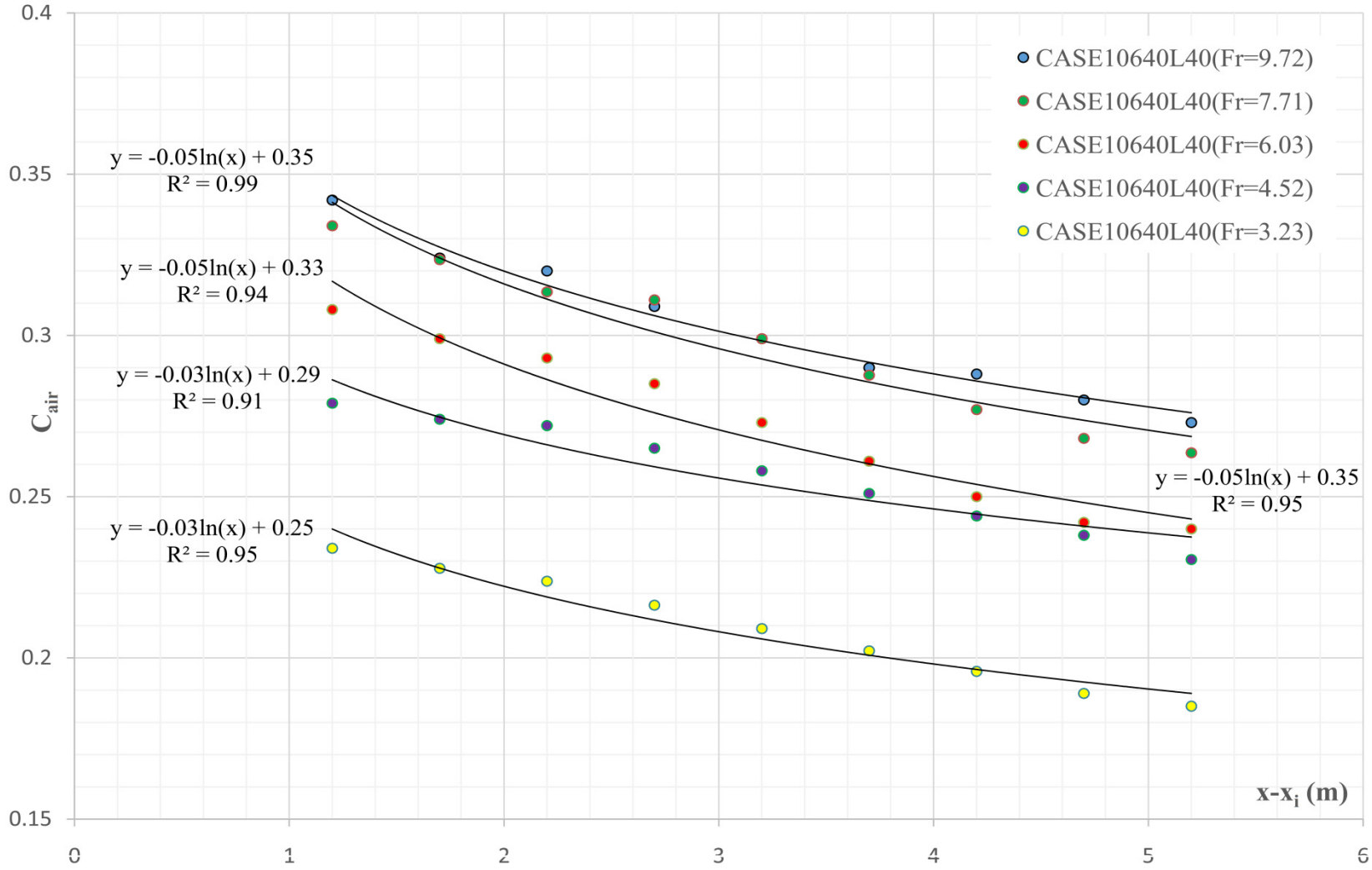

Figure 4.22: Cross sectional average air concentration at several streamwise locations for Cases 10640L40 with different *Fr*

4.8 Variation of Air Concentration over the Flow Depth

The variation of air concentration over the flow depth is investigated at two separate positions for the Cases00620L20, S20 and F20. The jet reattaches to the channel floor at around x_i=11 m in all three simulations. The concentration of the air below the free surface of the flow is calculated at x=15.5m and x=19.5m. The spanwise average air concentration values are plotted with respect to the flow depth ($z - z_o$) in Figures 4.23 and 4.24. The maximum air concentration appears approximately 40 cm away from the bottom at x=15.5 m (please see Figure 4.23). The location of the maximum air concentration moves away from the bottom as one goes to x=19.5 m (please see Figure 4.24). The plots show the variation of the air concentration until the free surface.

In literature the variation of air concentration with respect to the depth for flows over the steps that entrains air as it passes over the step without any other aeration duct is given with an analytical equation in Chanson (2013). This equation is based on the analytical solution of advection-diffusion equation of concentration. The concentration variation is given with a $\tanh^2$ function as in Equation 4.2.

$$C_{air} = 1 - tanh^2\left(A_1 - \frac{z-z_o}{2B_1} + \frac{(z-z_o-0.33)^3}{3B_1}\right) \quad (4.2)$$

In this equation A_1 is an integration constant, while B_1 is related to the air diffusivity. In the derivation of this equation the air entrainment in such flows are considered to be only from the upper nappe through the free surface. Therefore, the maximum concentration is known to be observed close to the free surface. However, in this study the aeration takes place at the lower nappe under the jet due to aeration ducts over the step, hence the equation that satisfies higher concentration values near the bed has a form given in Equation 4.3. In this equation A_2 is similar with A_1, B_2 is related to the diffusivity of the air in the flow in vertical direction similar to B_1 constant in Equation 4.2. C* could be expressed as a model coefficient that is used for fitting the analytical curve to numerical data.

$$C_{air} = C^* tanh^2\left(A_2 - \frac{z-z_o}{2B_2} + \frac{(z-z_o-0.33)^3}{3B_2}\right) \quad (4.3)$$

The analytical solution captures the trend reasonably well especially at locations closer to the reattachment point (please see Figure 4.23); however, due to various geometrical parameters, such as the shape of the air ducts and their location on the step, simulation results of variation of air concentration over the depth is not as symmetrical as given in the analytical curve. The maximum air concentration is observed at the centre of the air tubes and the location of the maximum concentration moves towards the free surface in the streamwise direction. The maximum air concentration is about 42% at x=15.5 m, while it is about 35% at x=19.5 m.

Below and above the maximum concentration depth, the air concentration values drop down however; air is still present close to the channel bottom even at further downstream locations. Scattered positioning of the ducts allows more homogenous air concentration values near the channel floor for S20 and F20 cases especially at upstream location (x=15.5 m) due to interpenetrating air tubes (please see Figure 4.23). The near bottom concentration values are also higher in these cases both at the upstream and downstream locations compared to L20. The air concentration at the channel floor is about 38-40% for S20 and F20 at x=15.5 m as opposed to 25% observed for L20. The air concentration decreases to 12-15% near the floor for cases S20 and F20 at x=19.5m while it decreases to 8% for L20 case as given in Figure 4.24. Analytical curve cannot capture the trend for these specific simulation conditions, especially close to the bed at the downstream locations which represented by dashed line in Figure 4.24.

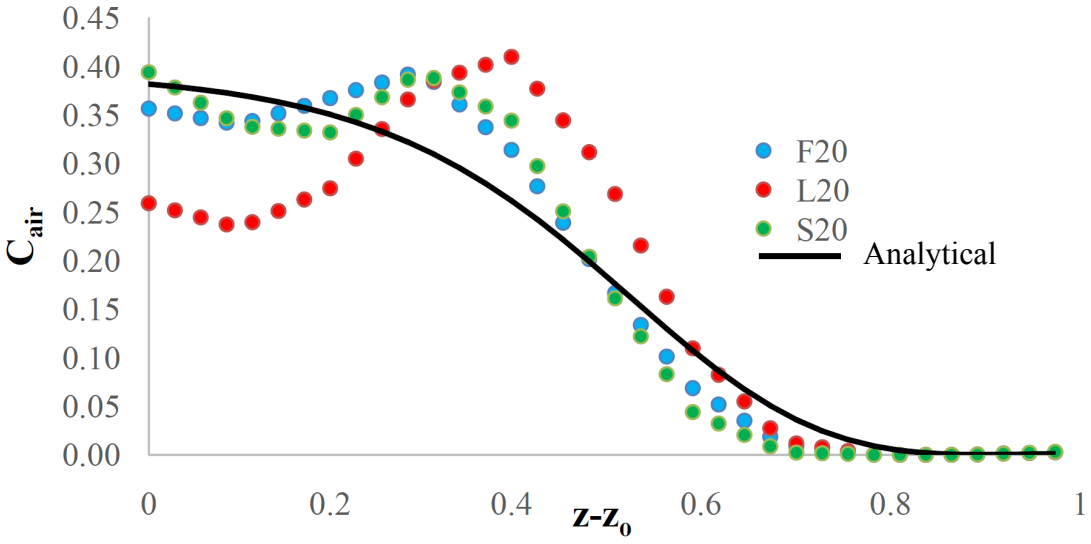

Figure 4.23: The spanwise average air concentration at x=15.5m for Cases 00620L20, S20 and F20

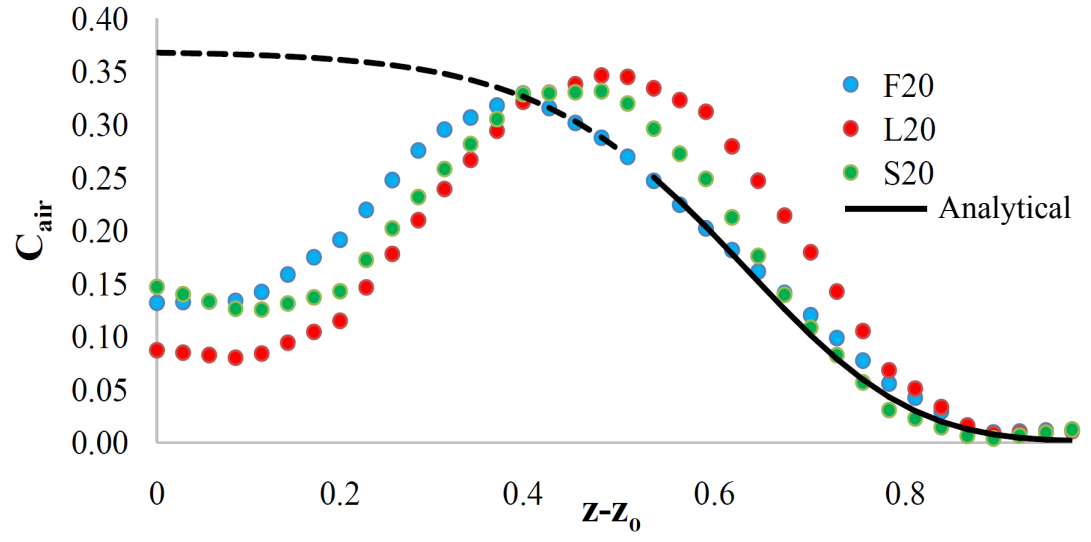

Figure 4.24: The spanwise average air concentration at x=19.5m for Cases 00620L20, S20 and F20

4.9 Summary of Results and Comparison with Previous Studies

In this section a brief summary of results are given. The tabulated form of the results of all 16 cases are given in Table 4.2. In the table h_{ramp} is the flow depth at the beginning of jet, V_{ramp} is the velocity of jet while leaving the chute over ramp, A_a is the total area of air ducts and A_w is the area of the flow calculated with h_{ramp}. Jet-lengths (L_j) are given in 3 columns for comparison with previous studies of Tan (1984) and Kökpınar and Göğüş (2002). The table also includes values for jet flight time (between leaving and reattachment) for present study and study of Tan (1984) and represented by "t_j". Another dimensionless constant "K"; which represents the relation between air entrainment and jet-length and used by many researchers, is calculated based on results of the current study. Comparison with previous studies is important for the validation of results. The result and application of the previous studies are explained briefly as a part of this section.

Table 4.2: Summary of results and comparison

Case	h_{ramp} (m)	V_{ramp} (m/s)	A_a/A_w	Froude Number	L_j (m) (Present Study)	L_j (m) (Kökpınar & Göğüş, 2002)	L_j (m) (Tan,1984)	t_j (s) (Present Study)	t_j (s) (Tan,1984)	β (%) (Present Study)	K
00620L20	1.10	18.2	0.03	5.53	6.45	5.00	5.61	0.35	0.30	16.95	0.029
00620S20	1.10	18.2	0.03	5.53	6.96	5.00	5.70	0.38	0.31	16.35	0.026
00620F20	1.10	18.2	0.03	5.53	6.65	5.00	5.65	0.37	0.30	16.50	0.027
00620L40	1.10	18.2	0.14	5.53	8.10	4.43	5.81	0.45	0.31	30.60	0.042
00620S40	1.10	18.2	0.14	5.53	7.27	4.43	5.76	0.40	0.31	27.99	0.042
10620L20	1.10	18.2	0.03	5.53	7.48	7.53	9.42	0.41	0.50	16.36	0.024
10620L40	1.10	18.2	0.14	5.53	10.10	6.68	9.43	0.56	0.50	48.37	0.053
10440L49	1.65	24.2	0.09	6.03	20.50	11.78	13.90	0.85	0.56	22.00	0.018
10340L57	1.65	24.2	0.09	6.03	21.55	11.78	13.90	0.89	0.56	21.60	0.017
10640L40(120)	1.20	33.3	0.13	9.72	24.20	22.12	22.00	0.73	0.64	33.45	0.017
10640L40(140)	1.40	28.6	0.11	7.71	20.00	16.31	17.58	0.70	0.60	29.60	0.021
10640L40	1.65	24.2	0.09	6.03	16.35	11.78	13.92	0.67	0.56	26.46	0.027
10640L40(200)	2.00	20.0	0.08	4.52	13.80	8.05	10.68	0.69	0.52	22.64	0.033
10640L40(250)	2.50	16.0	0.06	3.23	11.20	5.18	8.02	0.70	0.48	18.60	0.042
10670L40	2.70	25.9	0.06	5.04	17.90	11.84	15.19	0.69	0.57	17.25	0.026
20620L40	1.10	18.2	0.14	5.53	12.18	8.11	13.04	0.67	0.69	47.57	0.043

Study of Kökpınar and Göğüş (2002) is mainly focused on the jet flows over the spillway aerators. The aim of the study is to analyze the effect of geometric properties and flow conditions on jet-length and air entrainment capacity. Based on their experimental study and the results of the study of Demiröz (1985), some empirical formulas are developed by Kökpınar and Göğüş (2002).

$$\frac{L_j}{h_{ramp}} = 0.28(1+\alpha)^{0.22} Fr^{1.75} \left(\frac{t_r + H_s}{h_{ramp}} \right)^{0.44} \left[(1+\tan\theta) \frac{A_a}{A_w} \right]^{-0.087} \tag{4.4}$$

The limits of Equation 4.4 are $5.56 \le Fr \le 10.00,\ 0.198 \le (t_r + H_s)/h_{ramp} \le 1.985$, $0 \le \alpha \le 9.45°,\ 0 \le \tan\theta \le 1.25,\ 0.0684 \le A_a / A_w \le 1$, where A_a is total aeration area, A_w is area of flow over ramp or step, h_{ramp} is depth of flow over ramp or step and H_s is the step height measured perpendicularly from inclined channel bed. The cases of present study are within these limits. Jet-lengths given in Table 4.2 according to study of Kökpınar and Göğüş (2002) is calculated from the above equation. This equation does not account for the location of the aerator. Due to this, same jet-length values are calculated for the cases where only the locations of ducts are different. Jet-length obtained via Equation 4.4 is plotted against findings of the numerical simulations in Figure 4.25. The 45° angled dashed line shows case of full agreement between numerical and experimental findings which is hardly probable due to many factors. If a correction coefficient of 1.4 is applied to the empirical formula of Kökpınar and Göğüş (2002) a better agreement with R^2 =0.76 is obtained which is given as the solid line in Figure 4.25. This correction coefficient might be required due to scale effects that are commonly observed in physical experiments.

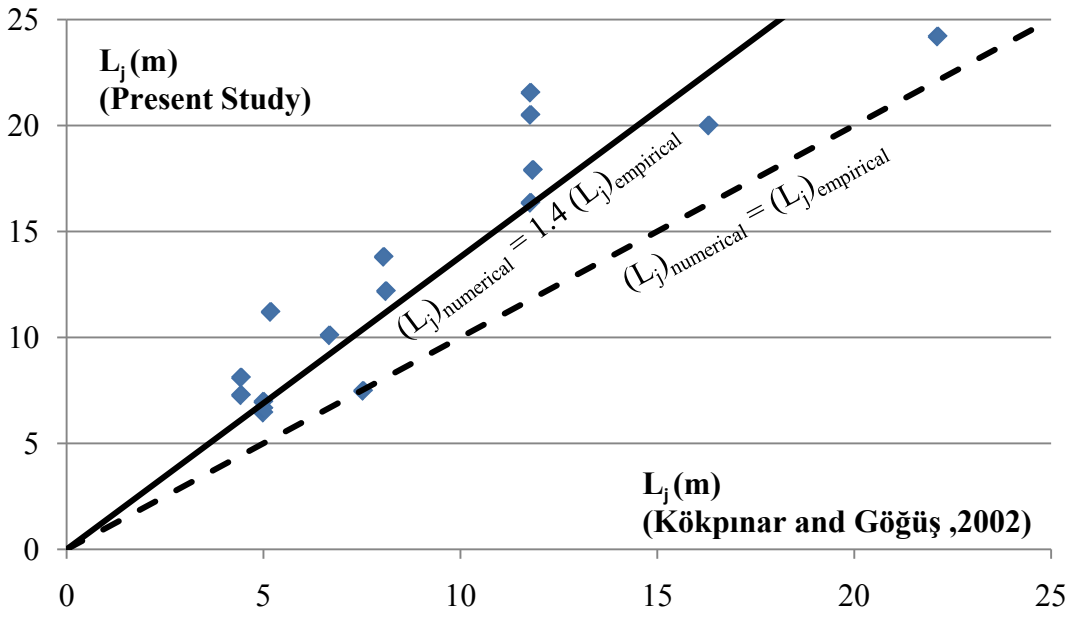

Figure 4.25: Jet-length plot for present study and study of Kökpınar and Göğüş (2002)

Study of Kökpınar and Göğüş (2002) also included a recommendation for aeration index β in the general form given in Equation 4.5 with respect to geometric properties of channel, flow depth and jet-length. Different from the findings of Kökpınar and Göğüş (2002), the best fit of this type of expression is obtained for the present study for cases with Froude number between 3.23-5.53 with the constant coefficients K_1, K_2 and K_3 are 0.06, 1.2 and 0.4, respectively. R^2 is found to be 0.91 with these coefficients. In the original equation from the experimental data set of Kökpınar and Göğüş (2002) these constants are, 0.0189, 0.83 and 0.24, respectively.

$$\beta = K_1 \left(\frac{L_j}{h_{ramp}} \right)^{K_2} \left[\left(\frac{A_a}{A_w} \right) (1 + \tan\theta) \right]^{K_3} \tag{4.5}$$

Tan's study published in 1984 is chosen for the further validation of results; because analytical recommendations of the study are based on geometric properties and a pressure term P_N, which is the cavity subpressure number. Inclusion of cavity subpressure number in the calculation of jet-length somehow accounts for the

location of the aerators, hence jet-length calculated using Tan's expression have varying values as the cavity subpressure number changes with the aerator location. Equations related to this study is given in Equations 4.6, 4.7 ,4.8 and 4.9. Equation 4.6 and 4.7 are for step ramp aerators and only step aerators, respectively for determining jet flight time. ΔP is the difference between atmospheric air pressure and lower nappe air pressure. In present study lower nappe air pressure value is obtained by reading pressure values at 100 points near the reattachment. These values are averaged to obtain cavity subpressure number. The jet-length based on Equation 4.9 is plotted against the current findings from the simulations in Figure Figure 4.26. Similar comments made for Figure 4.25 could be made for this figure. However, Tan's formulation based on pressure, estimates jet-length values closer to the present numerical results. Thus, the correction coefficient for this comparison is about 1.2 and the R^2 for the solid line is 0.86.

$$t_j = \frac{V_{ramp}\sin\alpha}{g\left(\cos\theta + P_N\right)}\left[1+\sqrt{1+2\left(t_r+H_s\right)\frac{g\left(\cos\theta+P_N\right)}{\left(V_{ramp}\sin\alpha\right)^2}}\right] \tag{4.6}$$

$$t_j = \sqrt{\frac{2H_s}{g\left(\cos\theta+P_N\right)}} \tag{4.7}$$

$$P_N = \frac{\Delta P}{\rho_w g h_{ramp}} \tag{4.8}$$

$$L_j = \frac{g\sin\theta}{2}t_j^2 + V_{ramp}(\cos\alpha)t_j \tag{4.9}$$

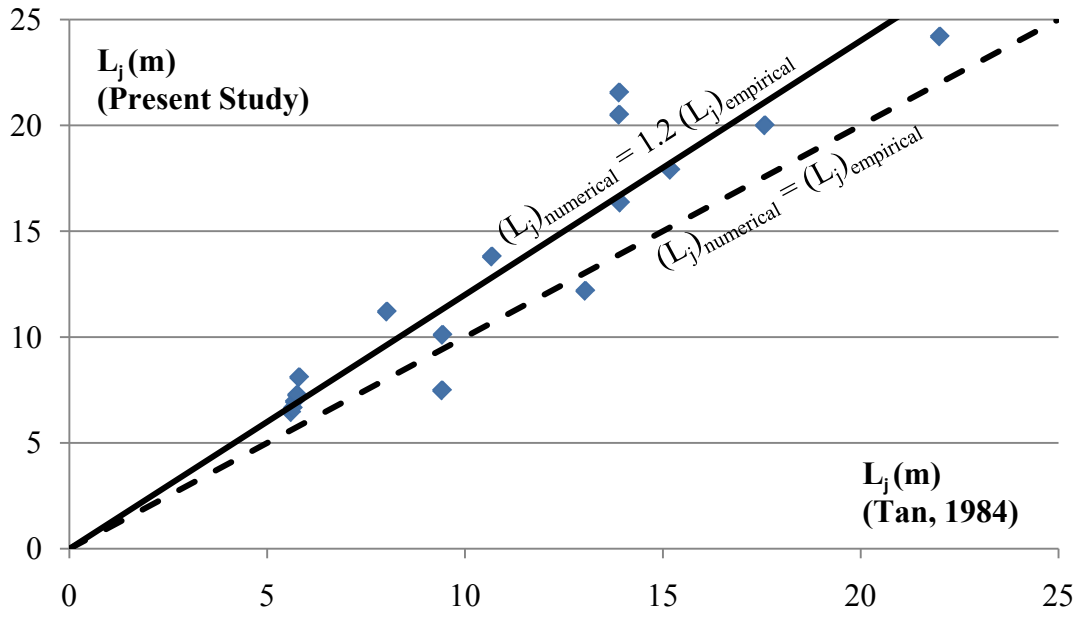

Figure 4.26: Jet-length plot for present study and study of Tan (1984)

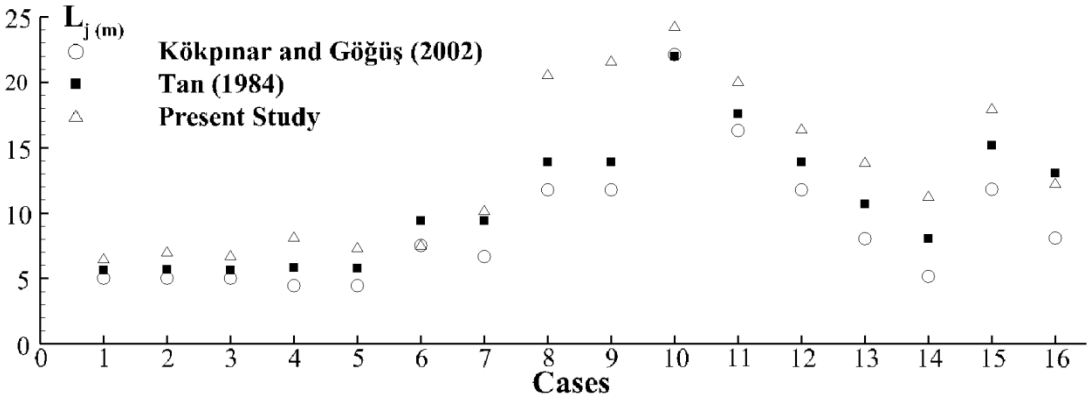

Figure 4.27: Jet-length calculated based on emprical formulas and jet-length observed through simulations for each case given in Table 4.2

The jet-length observed through numerical simulations are always somewhat larger than the values predicted by the empirical formulas of Tan (1984) and Kökpınar and Göğüş (2002) as seen in Figure 4.27. Kökpınar and Göğüş (2002) formulation

always predicts the jet-length shorter than present study and Tan (1984) formulation. However, the difference in values between Kökpınar and Göğüş (2002) and the present study is especially pronounced for cases 10440L49 and 10340L57. This might require further investigation of relation between number of aerators, total aeration area and jet-length.

The last comparison is related to the unitless number "K" proposed in previous studies. "K" term can be expressed by two different equations. First one is given as Equation 4.10 where q_a is air entrainment per meter chute width. Equation 4.11 is derived by substituting flow discharge per meter chute width, $q_w = V_{ramp} h_{ramp}$, in Equation 4.10. Table 4.3 shows present and previous values of "K". The values of "K" for present study is well in the range of previous studies.

$$q_a = K V_{ramp} L_j \tag{4.10}$$

$$\beta = K\left(\frac{L_j}{h_{ramp}}\right) \tag{4.11}$$

Table 4.3: "K" values for previous studies and present study

Study	K
Pinto et al. (1982)	0.023
Wei and DeFazio (1982)	0.01~0.035
Coleman et al. (1983)	0.02
Pinto and Neidert (1983)	0.01~0.08
Hamilton (1984)	0.01~0.05
Present Study	0.0165~0.0527

CHAPTER 5

CONCLUSION AND FUTURE WORK RECOMMENDATIONS

5.1 Conclusion

In the present study, flow characteristics near spillway aerators are investigated for submerged circular aerators considering various geometric parameters. The observed characteristics of the flow are mainly related with air entrainment phenomenon and jet-length of the flow from step to reattachment point. At the beginning of the study variables are chosen as discharge of the flow over spillway, aerators size, number and location, Froude number of flow, presence of a ramp and its angle. A three dimensional numerical model is used for studying mid to high discharge supercritical two-phase flow over a single slope spillway. Turbulence closure is via k-ε model and Volume of Fluid (VOF) method facilitates the air-water interface tracking.

A smooth convergence is observed in analyses with combination of VOF and k-ε model. Analyses are done for 1000 time steps, which corresponds to 10 flow-through time nearly for all cases. This amount of time is enough to reach steady state and for convergence. Observed jet-length values in this study are compared to the values retrieved through an empirical formula by Kökpınar and Göğüş (2002). This formula estimates the jet-length based on some geometric properties of channel. The estimated jet-length through this formula based on geometries of the present study agrees well with the observed jet-lengths in the simulations. Estimates from another empirical formula for jet-length by Tan (1984) is also used in order to compare the simulation results with the experimental ones available in literature. Different from empirical formula of Kökpınar and Göğüş (2002), Tan's formulation is based on

pressure values at the aeration zone. Better agreement between simulation results and the empirical estimates from Tan's formula is observed.

The "K" values obtained from this study are in the range of many previous studies. K value relates air and water discharge ratios of the flow to the relative jet-length. These validations suggest that average flow properties and behaviors of bottom aerated spillway flows could be studied and evaluated using three-dimensional numerical models that combines simple k-ε turbulence closure with VOF method.

The results of simulations show that for the flow discharge of $20 m^3/s/m$, the location of aerators does not have significant effect on air entrainment for the specific step size considered in this study. The aerator locations are taken as the only variable in Cases 00620L20, S20 and F20. In these simulations, at the approach of the step no ramp is present and the aerator size is taken as 20 cm. Scattered placed aerators are slightly more efficient in terms of increasing the jet-length compared to aerators located at far ends of the step. For this flow discharge and size of aerators, the values of β for all three cases are quite comparable. However relatively, the largest air entrainment is observed for L20 case where aerators are linearly placed even though the longest jet-length is observed for S20.

In the case of 40 cm diameter aerators with scattered placement, interpenetration of air tubes is observed. The air tubes form as the jet flows over the step and sucks the air through the circular ducts. In the Case 00620S40, two neighbouring air ducts work as one big air duct and in a sense total number of air ducts in the domain decreases. Even though, the air concentration near the channel floor might increase due to interaction of air tubes, the overall aeration of the flow decreases compared to L40 case. A similar observation is possible for Cases 10440L49 and 10340L57 where effect of number of air ducts is assessed. The results from these simulations are compared to Case 10640L40. In all three of these simulations, the total aeration area is identical. However, the number of aerators are different as the diameter of these aerators are larger in Cases 10440L49 and 10340L57 compared to Case 10640L40. With a decrease in number of aerators, about 4-5% decrease in β index is

observed. This might be due to decrease of suctioning effect of flow over larger diameter air ducts compared to aerators with smaller diameter. Interestingly, the jet-length increases much significantly with increase in aerator size while the number of aerators decreases in these cases.

Ramp height is also a variable in this study. For cases with aerators of 20 cm diameter, presence of a 10 cm high ramp offsets jet about 1 m however, in the terms of air entrainment no significant change is observed. For larger diameter (40 cm) cases presence of a 10 cm high ramp increases both jet-length and β values. Moreover, in the cases with larger diameter aerators, increase of ramp height from 10 cm to 20 cm only increases the jet-length but it has no significant effect on aeration.

Increase in discharge also increases the jet-length however, flow velocity is observed to have a greater role in the jet-length rather than the discharge itself. As it proposed in the study of Köpınar and Göğüş (2002) and seen in Figure 4.15, L_j / h_{ramp} is related with $Fr^{1.75}$.

The air entrainment depends both on L_j / h_{ramp} and A_a / A_w (ratio of total air entrainment area to flow area). Increase in diameter of aerators for same number of aerators, increases both jet-length and aeration ratio as expected.

By observing flow in the spanwise direction after reattachment point; it has been seen that placing smaller size aerators more frequently over the span of the spillway, generates wider protection zones with low flow velocities.

An expected result is decrease of average air concentration in the streamwise direction after reattachment of the flow. This decrease is found to be a logarithmic decay. The decay is somewhat faster for higher Froude number cases. The upward motion of air after the reattachment point in the streamwise direction is observed as expected due to difference between the specific gravity of water and air. This results in decrease of air concentration over the streamwise direction and increase of flow velocity near the channel floor. Following the analytical solution of Chanson (2013)

the spanwise average air concentration is expressed as $\tanh^2$ function of flow depth. The results show that such function might be more suitable near the jet reattachment, as the results deflect from such analytical expression as the flow propagates in the streamwise direction.

5.2 Future Work Recommendations

The results of this study could further be improved by considering other flow discharges, aerator sizes, aerator locations, aerator spacings in scattered configuration, ramp heights and step sizes. Much wider conclusions on effect of aerator size and location is possible by considering wider study range for these variables. A general formula on jet-length and air entrainment could be possible based on these variables with such a study.

In the present work, simple k-ε model is used for the turbulent flow calculations. In order to observe the turbulence related features of the flow, higher turbulence models such as detached eddy and large eddy simulation models could be used in the future. The shortcoming of k-ε model is that it calculates turbulent diffusion using a single turbulent length scale. This could be improved by using RNG variation of standard k-ε model, in which the dissipation equation tries to account for different length scales possible in a turbulent flow via using different model coefficients.

Furthermore, in this study a single set of aerators is analyzed for all cases. For complete design of a spillway, series of aerators should be used over the streamwise direction in order to prevent cavitation damages. CFD studies of cases with multiple aerator structures along the spillway could determine maximum allowable distance between the structures with sufficient aeration.

An optimization study for multiple aerators is also possible to determine the most economical array of aerators. Different type of aerator structures as given in Figure 1.1 could be considered in such work.

Another CFD study could look into the dynamics of a cavitation bubble formed over a spillway structure. This will help understanding nature of cavitation.

REFERENCES

Ansys, A. F. (2011). 14.0 Theory Guide. *ANSYS Inc.*, 390-1.

Arantes, E. J., Porto, R. M., Gulliver, J. S., Lima, A. C. M., & Schulz, H. E. (2010). Lower nappe aeration in smooth channels: experimental data and numerical simulation. *Annals of the Brazilian Academy of Science*, 82(2): 521-537.

Aydın, M. C. (2005). *CFD analyses of bottom-inlet spillway aerators*. PhD Thesis, Graduate School of Natural and Applied Sciences of Elazığ University, Elazığ.

Aydın, M.C., & Öztürk, M. (2009). Verification and validation of a computational fluid dynamics (CFD) model for air entrainment at spillway aerators. *Canadian Journal of Civil Engineering*, 36: 826-836.

Bhosekar, V. V., Jothiprakash, V., & Deolalikar, P. B. (2012). Orifice spillway aerator: Hydraulic design. *Journal of Hydraulic Engineering*, *138*(6), 563-572.

Cassidy, J. J., & Elder, R. A. (1984). Spillways of high dams. *Developments in hydraulic engineering-2, Edited by Novak, P., Elsevier Applied Science Publishers Ltd.*, Essex, England, 159-182.

Chanson, H. (1990). Study of air demand on spillway aerator. *Journal of Fluids Engineering*, *112*(3), 343-350.

Chanson, H. (2013). Advective Diffusion of air bubles in turbulent water flows. *Fluid mechanics of environmental interfaces, Edited by Gualtieri, C. and Mihailovic, D. T., CRC Press*, 181-219.

Coleman, H., Simpson, A., & de Garcia, L. (1983). Aeration for cavitation protection of Uribante Spillway. In *American Society of Civil Engineers, Hydraulics Division Specialty Conference, Frontiers in Hydraulic Engineering (1983: Cambridge, Massachusetts, USA)*.

Demiröz E., Darama Y., & Kuzum L. (1994). Study of the effectiveness of the aerators placed on the spillway chutes of Keban Dam. In *Commission Internationale Des Grands Barrages, 18'Congres Des Barrages, Durban,* 353-367.

Demiröz, E. & Darama Y. (1992). A comparative study between the study between the prototype and laboratory data of the aerators placed on the spillway discharge channels of the Keban Dam. *International Symposium on Hydraulic Research in Nature and Laboratory.* Wuhan,China.

Demiröz, E. (1985). Spillway aerator project criterions used for high-speed chute flows, *TÜBİTAK*, Engineering Research Group, Project 606, Ankara

Hamilton, W. S. (1983). Preventing cavitation damage to hydraulic structures. *International water power & dam construction*, *35*(12), 48-53.

Kells, J. A., & Smith, C. D. (1991). Reduction of cavitation ın spillways by induced air entrainment. *Canadian Journal of Civil Engineering*, 18(3): 358-377.

Kökpınar, M. A. & Göğüş, M. (2002). High-speed jet flows over spillway aerators. *Canadian Journal of Civil Engineering*, 29: 885-898.

Kökpınar, M. A. (2004). Deriner Barajı dolusavak havalandırıcıları modeli nihai rapor, *DSİ Teknik araştırma ve Kalite Kontrol Dairesi Başkanlığı*, Yayın No: Hİ-965, Model No: M-359. Ankara, 100s.

Kramer, K. (2004). *Development of aerated chute flow*. PhD Thesis, Swiss Federal Instıtute of Technology Zurich, ETH Zürich.

Kramer, K., Hager, W. H., & Minor, H. E. (2006). Development of air concentration on chute spillways. *Journal of Hydraulic Engineering*, *132*(9), 908-915.

Launder, B. E., & Spalding, D.B. (1972). Lectures in mathematical models of turbulence. Academic Press, London, England.

Lee, W., & Hoopes, J. A. (1996). Prediction of cavitation damage for spillways.*Journal of Hydraulic Engineering*, *122*(9), 481-488.

Lesleighter, E. J. (1988). Cavitation in hydraulic structures. In *Model-Prototype Correlation of Hydraulic Structures,* Colorado Springs, Colorado, 74-94.

Lesleighter, E. J., & Chang, H. T. (1981). Experience on flow aeration to prevent cavitation erosion in spillway chutes. In *Conference on Hydraulics in Civil Engineering 1981: Preprints of Papers* (p. 128). Institution of Engineers, Australia.

Markatos, N. C. (1986). The mathematical modeling of turbulent flows. *Applied Mathematical Modeling*, *10*(3), 190-220.

Nguyen, C. (2005). Turbulence Modeling. *Cambridge: Department of Aeronautics and Astronautics. Available through: Massachusetts Institute of Technology http://www.mit.edu/cuongng/Site/Publicationfiles/TurbulenceModeling04NOV05. pdf [Accessed 5 September 2015]*.

Oskolkov, A. G., & Semenkov, V. M. (1979). Experience in designing and maintenance of spillway structures on large rivers in the USSR. In *Thirteenth International Congress on large dam, New Delhi. India, Q* (Vol. 50, pp. 789-802).

Pan, S., Shao, Y., Shi, Q.; & Dong, X. (1980). The self-aeration capacity of the water jet over the aeration ramp. *Shuili Xuebao (Journal of Hydraulic Engineering)*, Beijing, PRC, 5: 13-22. (USBR Translations, Denver, Colo., Fevruary 1983.)

Pinto, N. L. S. (1988). Cavitation and aeration, *Advanced dam engineering for design, construction and rehabilitation.* Kluver Academic Publishers, Jansen, RB, 620-634.

Pinto, N. L. S., & Neidert, S. H. (1983). Evaluating entrained air flow through aerators. *Water Power and Dam Construction*, *35*, 40-2.

Pinto, N. L. S., Neidert, S., & Ota, J. J. (1982). Aeration at high velocity flows, *Water Power and Dam Construction*, 34(2): 34-38; 34(3):42-44.

Rutschmann, P., & Hager, H. (1990). Air entrainment by spillway aerators. *ASCE Journal of Hydraulic Engineering*, 116(6): 765-782.

Schwartz, I., & Nutt, L.P. (1963). Projected nappes subjected to transverse pressure. *ASCE Journal of Hydraulics Division*, 89(7), 97-104.

Tan, T. P. (1984). *Model studies of aerators on spillways*. Research Report 85-6, Department of Civil Engineering, University of Canterbury, Christchuch, New Zealand.

Tennekes, H., & Lumley, J. L. (1972). *A first course in turbulence*. MIT press.

Volkart, P., & Chervet, A. (1983). *Air slots for flow aeration: determination of shape, size and spacing of air slots for the San Roque Dam spillway*. Versuchsanstalt für Wasserbau, Hydrologie und Glaziologie.

Volkart, P., & Rutschmann, P. (1984). *Air entrainment devices (air slots)*. Versuchsanst. für Wasserbau, Hydrologie und Glaziologie.

Volkart, P., & Rutschmann, P. (1991). Aerators on spillways. *IAHR hydraulic structures design manual*, *4*, Air entrainment in free-surface flows, 85-113, Rotterdam.

Wei, C. Y., & DeFazio, F. G. (1982). Simulation of free jet trajectories for the design of aeration devices on hydraulic structures. In *Finite Elements in Water Resources* (pp. 1039-1048). Springer Berlin Heidelberg.